Featuring work from Luciano De Sio at Sapienza University of Rome, and Francesca Petronella at National Research Council, Italy.

Label-free and reusable antibody-functionalized gold nanorod arrays for the rapid detection of *Escherichia coli* cells in a water dispersion

Early warning systems that monitor the quality of drinkable water are crucial to protect people's health. A reusable, real-time, and miniaturized biosensor is presented using the sensitivity and the multicolor thermoplasmonic properties of antibody functionalized gold nanorod arrays.

As featured in:

See Francesca Petronella, Luciano De Sio *et al.*, *Environ. Sci.: Nano*, 2022, **9**, 3343.

ROYAL SOCIETY OF **CHEMISTRY**

rsc.li/es-nano

PAPER

Check for updates

Label-free and reusable antibody-functionalized gold nanorod arrays for the rapid detection of *Escherichia coli* cells in a water dispersion†

Francesca Petronella, [iD] *[a] Daniela De Biase, [iD] [b] Federica Zaccagnini,[b] Vanessa Verrina,[b] Seok-In Lim,[c] Kwang-Un Jeong, [iD] [c] Selenia Miglietta,[d] Vincenzo Petrozza,[b] Viviana Scognamiglio,[a] Nicholas P. Godman,[e] Dean R. Evans,[e] Michael McConney[e] and Luciano De Sio [iD] *[bf]

The growing spread of pathogens, caused by anthropogenic activities, pushes the interest of the scientific community towards developing biosensors with improved performance for rapid, simple, and on-site pathogen detection. In this study, we present and discuss a label-free gold nanorod (Au NR) array for the rapid detection of *Escherichia coli* cells in water, resulting in an effective optical transducer, based on the phenomenon of localized surface plasmon resonance (LSPR). Au NRs with different aspect ratios are functionalized with a suitable antibody by an electrostatic-linking method, resulting in two different Au NR-based bioconjugates. We investigate the ability of the two bioconjugates to detect and spectroscopically recognize *E. coli* cells dispersed in water by specific antigen–antibody interaction. The results allow selecting the Au NR morphology more suited for preparing the Au NR bioactive array on a glass substrate with excellent optical and morphological properties. The antibody-functionalized Au NR array can detect *E. coli* cells with high sensitivity and a limit of detection of 8.4 CFU mL^{-1}, resulting in an excellent label-free spectroscopic biosensor. In addition, the multicolor thermoplasmonic properties of the Au NR array, triggered by appropriate light sources, are suited to enable on-demand photothermal disinfection, thus providing an extraordinary capacity for the biosensor to be both disinfected and, more importantly, reutilized.

Environmental significance

Microbial contamination of water produces relevant human-health problems, spanning from infectious diseases to biosecurity. Currently available techniques for pathogen detection require a long workflow, specialized personnel, and considerable waste. This manuscript reports a breakthrough in monitoring microbial contamination by developing a fast, user-friendly, compact, and reusable *in situ* biosensor to detect pathogens in water. The nano-inspired device uses an antibody-functionalized Au NR array for identifying and quantifying *Escherichia coli*. It exhibits a limit of detection of 8.4 CFU mL^{-1}, which turns out to be one order of magnitude lower than that of conventional plasmonic biosensors. In addition, the photothermal properties of the Au NR array are investigated to enable on-demand photothermal disinfection, thus providing reusability and sustainability.

[a] Institute of Crystallography CNR-IC, National Research Council of Italy, Via Salaria Km 29,300, Monterotondo - Rome, Italy. E-mail: francesca.petronella@ic.cnr.it

[b] Department of Medico-Surgical Sciences and, Biotechnologies Sapienza University of Rome, Latina, Italy. E-mail: luciano.desio@uniroma1.it

[c] Department of Polymer-Nano Science and Technology, Department of Nano Convergence Engineering, Jeonbuk National University, Jeonju, Republic of Korea

[d] Department of Anatomy, Histology, Forensic Medicine and Orthopaedics, Sapienza University of Rome, Rome, Italy

[e] Air Force Research Laboratory, Materials and Manufacturing Directorate, Wright-Patterson Air Force Base, Ohio, 45433, USA

[f] Center for Biophotonics Research, Department of Medico-Surgical Sciences and Biotechnologies, Sapienza University of Rome, Latina, Italy

† Electronic supplementary information (ESI) available. See DOI: **https://doi.org/10.1039/d2en00564f**

Introduction

The Covid 19 pandemic has demonstrated how the growing spread of pathogens burdens human health, environmental ecosystems, and human security. Contaminated water is one of the primary sources of pathogen transmission, and the World Health Organization (WHO) estimated 485 000 diarrheal deaths each year, ascribable to contaminated drinking water.[1] Anthropogenic causes including the misuse of wastewater reuse plants,[2] frequent heavy rainfall caused by global warming,[3,4] and the growing diffusion of plastic waste and microplastics, where microorganisms attach and form biofilms,[5,6] increase the proliferation, survival, transport, and dispersal of human pathogens in water. In addition, water

This journal is © The Royal Society of Chemistry 2022

Environ. Sci.: Nano, 2022, **9**, 3343–3360 | **3343**

reservoirs represent potential targets for terroristic activity worldwide because of the critical role that drinkable water plays in our everyday lives. Intentional contamination of municipal water systems with biological agents or "bioweapons" as part of a terrorist attack would lead to serious public health issues and has a significant psychological impact on people's lives and economic consequences.[7] For these reasons, early warning systems are now imperative for timely water contamination monitoring to ensure inclusive public health and minimize the risk of waterborne disease outbreaks. Mainstream techniques for pathogen detection, such as polymerase chain reaction (PCR)-based and immunology-based methods, require a complex workflow, expensive equipment, specialized personnel, and massive reagent consumption. Culture-based processes, considered as the gold standard for pathogen identification and monitoring, although simple, are time-consuming[8] and poorly sustainable from an environmental standpoint, as they require a large amount of disposable laboratory plasticware, generating a massive amount of plastic waste.[9]

Biosensors are a promising tool to outclass conventional analytical techniques. They ensure constant monitoring and rapid response times, sensitivity, and selectivity and minimize sample pretreatment processes.[8,10] Nanotechnology offers a ground-breaking toolbox for designing and fabricating miniaturized biosensors suitable for point of-care, end of-use, and sampling applications. Advanced nano-biosensor design and fabrication opportunities are offered by plasmonic gold nanoparticles (Au NPs).[11] Au NPs exhibit optimal colloidal stability, effective interaction with biomolecules, easy processable surface chemistry, high electron density, and unique optical properties.[12] The optical properties of Au NPs are associated with the localized surface plasmon resonance (LSPR) phenomenon, *i.e.*, the collective oscillation of electrons localized at the metallic/dielectric interface produced by suitable light irradiation. The LSPR generates sharp and intense absorption peaks (plasmons) in the visible/near-infrared (NIR) range of the electromagnetic spectrum, whose frequency and profile are strongly dependent on the specific morphology and surface chemistry of Au NPs, described by the Mie and Gans theory.[13,14] In addition, the LSPR frequency is susceptible to the local refractive index (n) change.[15] Such a relation is the physical basis underlying LSPR biosensing, making Au NPs excellent optical transducers for monitoring the local change of the surrounding medium.[15] The general scheme of Au NP-based LSPR biosensors consists of Au NPs appropriately functionalized with a biorecognition element, including antibodies, aptamers, peptides, DNA, and bacteriophages, resulting in a bioconjugate.[16] In the presence of the specific target bio-entity, the biorecognition element triggers an interaction with the surface of Au NPs that alters the local n, thus inducing an optical shift (a change of the LSPR frequency) in the absorption spectrum of Au NPs.[17] LSPR biosensors for spectroscopic recognition of pathogens can provide real-time, quantitative detection, with high sensitivity and selectivity, which makes them extremely appealing for developing early-

warning, compact, and portable sensing platforms.[15,17] However, a step forward is needed to realize functional Au NP arrays on substrates to be integrated into optical devices for the development of LSPR spectroscopic biosensors. Recently, Au NP arrays were employed for the optical detection of pathogens. *Salmonella typhimurium* was detected in food samples using an LSPR biosensor consisting of a monolayer of Au NPs self-assembled on a glass substrate and then functionalized with an aptamer.[18] *S. typhimurium* was also detected by an Ω-shaped fiber-optic LSPR biosensor, using an array of Au NPs functionalized with a suitable aptamer as an optical transducer.[19] In a different approach, a fiber-optic functionalized with Au NPs was created to capture, recognize and quantify *E. coli* cells using a bacteriophage as a biorecognition element.[20] An LSPR biosensor based on an array of Au NPs was also developed to monitor the kinetics of *E. coli* biofilm generation.[21] Although robust and reliable, currently available LSPR biosensors, displaying a limit of detection (LOD) in a range from 10^2 and 10^4 CFU mL^{-1},[18,19] are still unsuitable for real-time monitoring of pathogens in water. In light of WHO and European Union requirements, imposing no *E. coli* cells in 100 mL of water,[22] more efforts are needed to design and realize LSPR biosensors with superior performance.

The present work tackles this challenge by designing and realizing a miniaturized, label-free, antibody-functionalized Au NR array on a glass substrate to rapidly detect *E. coli* cells in water with improved sensitivity. To accomplish the desired sensing performance, rod-like Au NPs (Au NRs) were selected as *E. coli* LSPR probes instead of the spherical Au NPs conventionally used to fabricate sensing platforms.

The anisotropic morphology of Au NRs results in an absorption spectrum characterized by two LSPR bands: the transverse plasmon (LSPRt) typically centered at 520 nm and the longitudinal plasmon (LSPRl), centered at higher wavelengths and tunable according to the Au NR aspect ratio. Remarkably, the LSPRl is more sensitive to n alterations with respect to the LSPRt;[15] indeed, several Au NR bioconjugates were used in colloidal LSPR sensors for spectroscopic detection of pathogens.[23–25] In this study a novel bioactive array of Au NRs with optimal optical and morphological properties for LSPR biosensing of a model pathogen, *E. coli*, was developed. As a first step, the biosensing performance of two bioconjugates prepared with Au NRs at different aspect ratios was investigated to determine the more effective Au NR morphology for *E. coli* LSPR biosensing. The two Au NR-based bioconjugates were functionalized with a suitable antibody (anti-*E. coli* Ab or Ab) able to target surface antigens of *E. coli*. The bioconjugation was realized by modifying an electrostatic linking method[26–28] that allows promoting the electrostatic attractions between the Au NR surface and the anti-*E. coli* Ab by interposing a polyelectrolyte (PE) layer, namely a polymer carrying numerous charged (ionizable) groups, resulting in a polycation or a polyanion.[28] The two bioconjugates were carefully characterized and their ability to spectroscopically recognize and quantify *E. coli* cells in water dispersions was investigated. Based on experimental results, the Au NR

morphology more suited for preparing Au NR-based bioactive substrates was identified. The substrates were realized by exploiting the electrostatic layer-by-layer (LbL) assembly method,[30,31] characterized both from an optical and a morphological point of view, (bio)activated by incorporating the anti-E. coli Abs by physisorption, and finally investigated for the recognition and quantification of E. coli cells dispersed in water. In addition, a multicolour thermoplasmonic investigation was performed to assess the capability of the substrates to be photothermally disinfected and reutilized.

Experimental

Materials

Citrate-capped gold nanorods (40 nm × 15 nm, Au NR 660) and Au NRs (55 nm × 15 nm, Au NR 800) were purchased from Nanocomposix. Poly(sodium 4-styrenesulfonate) (PSS, Mw ~70 kDa), and poly(allylamine hydrochloride) (PAH, Mw ~50 kDa), acetone, isopropanol methanol, sodium hydroxide (NaOH), and liquid crystal E7 were purchased from Merck. The mouse monoclonal antibody E. coli (1011):sc-57709 (anti-E. coli Ab or Ab) was purchased from Santa Cruz Biotechnology, Inc. Deionized water was used in all the procedures. The bacterial E. coli K12 strain MG1655 CGSC#7740 was obtained from the Coli Genetic Stock Centre (CGSC) collection. The growth of bacteria was carried out in chemically defined minimal medium E supplemented with 0.4% glucose. Chemicals for bacterial growth were purchased from Merck or VWR International. The fluorescent dyes SYTO 9™ and propidium iodide, used for detection of E. coli cells by fluorescence microscopy, were purchased from Thermo Fisher Scientific.

Bioconjugation of Au NRs with antibody

The Au NR–Ab-based bioconjugates were obtained by suitably modifying the protocol reported in ref. 26. The procedure consists of the first step of Au NR functionalization with PAH and the second step of bioconjugation with the Ab. First, commercial dispersions of pristine Au NRs were concentrated four times, resulting in two colloidal dispersions of Au NR 660 (4×) and Au NR 800 (4×). Next, a defined volume of PAH stock solution (10 mg mL^{-1} prepared in 10 mM NaCl solution, pH 2) was introduced in both the Au NR (4×) dispersions (40 μL for Au NR 660 (4×) and 100 μL for Au NR 800 (4×)). After adding 50 μL of 10 mM NaCl, the resulting mixtures were kept for 30 min under vigorous magnetic stirring. At this stage, excess PAH was removed by centrifugation (14 000 rpm, 8 min, 4 °C), and the two pellets were redispersed in 1.2 mL of deionized water, resulting in Au NR 660/PAH and Au NR 800/PAH colloidal dispersions. Finally, 60 μL of Ab stock solution (0.1 mg mL^{-1}) was added to both Au NR 660/PAH and Au NR 800/PAH, and the two dispersions were left to incubate for 30 min under magnetic stirring at room temperature to induce the electrostatic linkage mediated by the PAH. The resulting bioconjugates Au NR 660/PAH/Ab and Au NR 800/PAH/Ab were isolated by centrifugation (14 000 rpm, 15 min, 4 °C) and redispersed in water for further stud-

ies. The concentrations of Au NR 660/PAH/Ab and Au NR 800/PAH/Ab were suitably adjusted to achieve the same optical density of 0.5 absorption units.

Fabrication of Au NR-based substrates

Immobilization of Au NRs. The experimental procedure for the fabrication of glass substrates hosting Au NRs was performed by suitably modifying the protocol described in ref. 32. The procedure consists of several steps, including the washing of the glass substrates, the modification of the glass substrates by introducing a negative charge, the building of the PE multilayer and, finally, the immobilization of Au NRs. The glass substrates of 1 cm × 1 cm in size were cleaned by sequential sonication for 10 min in methanol and acetone baths followed by an intermediate rinsing step in isopropanol. Afterward, the cleaned slides were dried under a stream of nitrogen. To induce a negative charge on the glass surface, the substrates were immersed for 30 min in a solution of 5 M NaOH and rinsed with water. After that, the negatively charged glass substrates were modified with the PE multilayer by assembling the sequence PAH/PSS/PAH. Each substrate was immersed for 10 min in a 1.6 mg mL^{-1} PAH aqueous solution at pH 2. The PAH-modified substrates were then immersed in water for 2 min to remove excess PAH and next immersed in the PSS solution (1.6 mg mL^{-1}, pH 8) for 10 min. After that, the substrates were rinsed with water by immersion for 2 min, and a final layer of PAH was deposited. The incorporation of Au NRs was achieved by immersing the PE-modified glass substrate in a dispersion of Au NRs with an optical density of 1 (at 790 nm) for 16 h. At this stage, the substrates were rinsed with water, dried under a nitrogen stream, and used for optical and morphological characterization.

Au NR-based substrate functionalization. The array of Au NRs on the glass substrate was (bio)functionalized with Ab 1011 by physisorption. Briefly, each Au NR-based substrate was immersed for 2 h in a water solution of Ab 1011 with a concentration of 0.01 mg mL^{-1}, rinsed with water, and gently dried under a nitrogen stream, resulting in an active Au NR-modified substrate for the subsequent characterization and experiments.

Sensitivity to refractive index changes. To investigate the optical response of the Au NR-based substrates as a function of the local n, different glass cells were fabricated. NOA-61 (containing well-monodispersed 10 μm glass microbeads) was deposited at the corners of the substrate before covering the Au NR-based substrates with glass slides. The cells were sealed by a 1 min UV exposure, thus resulting in a gap 10 μm thick. The resulting gap was infiltrated with 50 μL of the solutions at different n values, including water, olive oil, NOA-61, and nematic liquid crystal E7 (NLC). The cell prepared for the NLC sample was made with a modified top glass substrate for promoting the planar alignment of the NLC film. The different media were allowed to penetrate the sample for 2 min to promote a uniform and complete distribution of the

This journal is © The Royal Society of Chemistry 2022

Environ. Sci.: Nano, 2022, **9**, 3343–3360 | **3345**

solution within the cell. Finally, the optical response was evaluated by collecting the absorption spectra.

Spectroscopic detection of *E. coli* cells in water dispersions. To assess the ability of Au NR 660/PAH/Ab and Au NR 800/PAH/Ab to recognize *E. coli* cells in water dispersions, an absorption spectroscopy assay was performed. In particular, aliquots from a 10^3 CFU mL^{-1} water dispersion of *E. coli* were progressively added to both Au NR 660/PAH/Ab and Au NR 800/PAH/Ab bioconjugates, and the respective absorption spectrum was collected. After adding each aliquot and collecting the absorption spectra, the system was left to stir for 10 minutes to promote the antigen/antibody interactions. Experimental data were analyzed by plotting, for each bioconjugate, the optical shift as a function of *E. coli* concentration expressed in CFU mL^{-1}. The optical shift ($\Delta\lambda = \lambda_f - \lambda_i$) was calculated as the difference between the wavelength position of the LSPRl of the bioconjugate after the introduction of each *E. coli* aliquot (λ_f) and the wavelength of the LSPRl of the as-prepared bioconjugate (λ_i). The LOD was evaluated as three times the standard deviation of the intercept calculated from the linear interpolation of the $\Delta\lambda$ values as a function of *E. coli* concentration.[33,34]

Control experiments were performed applying the same protocol for pristine Au NR 660, Au NR 800, Au NR 660/PAH, and Au NR 800/PAH.

Spectroscopic detection of *E. coli* cells on Au NR-based glass substrates. The ability of Au NR-modified substrates functionalized with the Ab to accumulate and recognize *E. coli* cells was investigated. The Au NR substrates bioactivated with the Ab were incubated in 500 μL *E. coli* dispersion (in minimal E) for 20 min in a range of concentrations from 10 CFU mL^{-1} to 10^4 CFU mL^{-1}. Then, 2 μL of the fluorescent dye SYTO 9™ was added to the solution, and the sample was left to immerse for an additional 10 min in the dark. After incubation, the substrates were immersed in 600 μL of water for 1.5 min to remove the excess of both *E. coli* cells and SYTO 9™ and gently dried. Control experiments were performed by using unfunctionalized Au NR substrates and by incubating the bioactive substrates in 500 μL of minimal E for 20 min and then introducing 2 μL of the fluorescent dye SYTO 9™ followed by washing and drying steps before the acquisition of the absorption spectrum. Other control experiments were performed, and all the details and results are well described in the ESI.†

Bacteria culture. The reference *E. coli* laboratory strain used in this study is *E. coli* K12 strain MG1655. The chemically defined minimal medium A or minimal medium E supplemented with 0.2% and 0.4% glucose, respectively, was used in this study for the *E. coli* growth. Briefly, a few colonies of *E. coli* from a freshly streaked plate were transferred into 30 ml of chemically defined medium in a 250 ml Erlenmeyer flask and allowed to grow overnight at 37 °C under orbital shaking. The culture was then centrifuged at 8000g for 15 min, the spent medium was discarded, and the bacterial pellet was resuspended in 20 ml of physiological solution (0.9% NaCl). The *E. coli* growth was monitored by determining the optical density at 600 nm (OD$_{600}$). The optical density

was measured, and an aliquot of the bacteria was further diluted in the growth medium to 1×10^7 CFU ml^{-1}.

Sample characterization

UV-visible absorption spectroscopy. UV-visible absorption spectroscopy studies for the optical characterization of the Au NR-based bioconjugates and the Au NR-based substrates were performed by using a Lambda 365 spectrophotometer from PerkinElmer. The *E. coli* growth was monitored by determining the OD$_{600}$ by using a diode array spectrophotometer (HP8453; Agilent Technologies).

Photoluminescence spectroscopy. Photoluminescence spectra were recorded by using a FP-8200 spectrofluorometer (Jasco). All measurements were performed at room temperature.

Transmission electron microscopy. TEM micrographs were obtained using a Carl Zeiss EM10 TEM (Carl Zeiss, NY, USA) operating at 60 kV voltage with a DEBEN XR80 AMT CCD camera (Deben, Melton).[35,36] One drop (10 μL) of each sample was cast on a carbon-coated copper grid and allowed to dry before the analysis.

Atomic force microscopy. The surface profile was investigated by atomic force microscopy (AFM, Nanoscope Multimode system, Veeco Instruments) in tapping mode. The vertical resolution is 0.1 Å and the lateral resolution is 2 Å.

Scanning electron microscopy. Scanning electron microscopy (SEM) micrographs were obtained by field emission scanning electron microscopy (FE-SEM, Carl Zeiss, SUPRA 40VP) to investigate the morphology of the substrate covered by Au NR 800 nm. The accelerating voltage is 2.00 kV.

Multicolour photothermal measurements. For evaluating the photothermal properties of the Au NR 800 array on the glass substrate, a two-color thermo-optical setup was implemented. The thermo-optical setup uses a CW diode laser (Laser Quantum) operating at 532 nm and a CW diode laser (Coherent Powerline) operating at 808 nm. The schematic representation of the two-color thermo-optical setup is sketched in Fig. 6a. The green laser has a circular spot. The near-infrared laser beam has a rectangular profile, which was converted into an almost circular spot utilizing a 20 cm focal length elliptical lens. A high-resolution thermal camera (FLIR, A655sc) was used to map and identify the spatial heating distribution and temperature profile under lateral pumping laser illumination. The camera produces thermal images of 640 × 480 pixels with an accuracy of ±0.2 °C. It works seamlessly with proprietary software (FLIR ResearchIR Max) to record and process the thermal data acquired by the camera.

Photothermal disinfection. For evaluating the ability of the Au NR 800 array on the glass substrate to achieve photothermal disinfection of *E. coli* cells, the thermo-optical setup described in the section "Multicolour photothermal measurements" was used. In particular, only the CW diode laser operating at 808 nm irradiated the sample. After the biofunctionalization step, the bioactive substrate Au NR 800/Ab
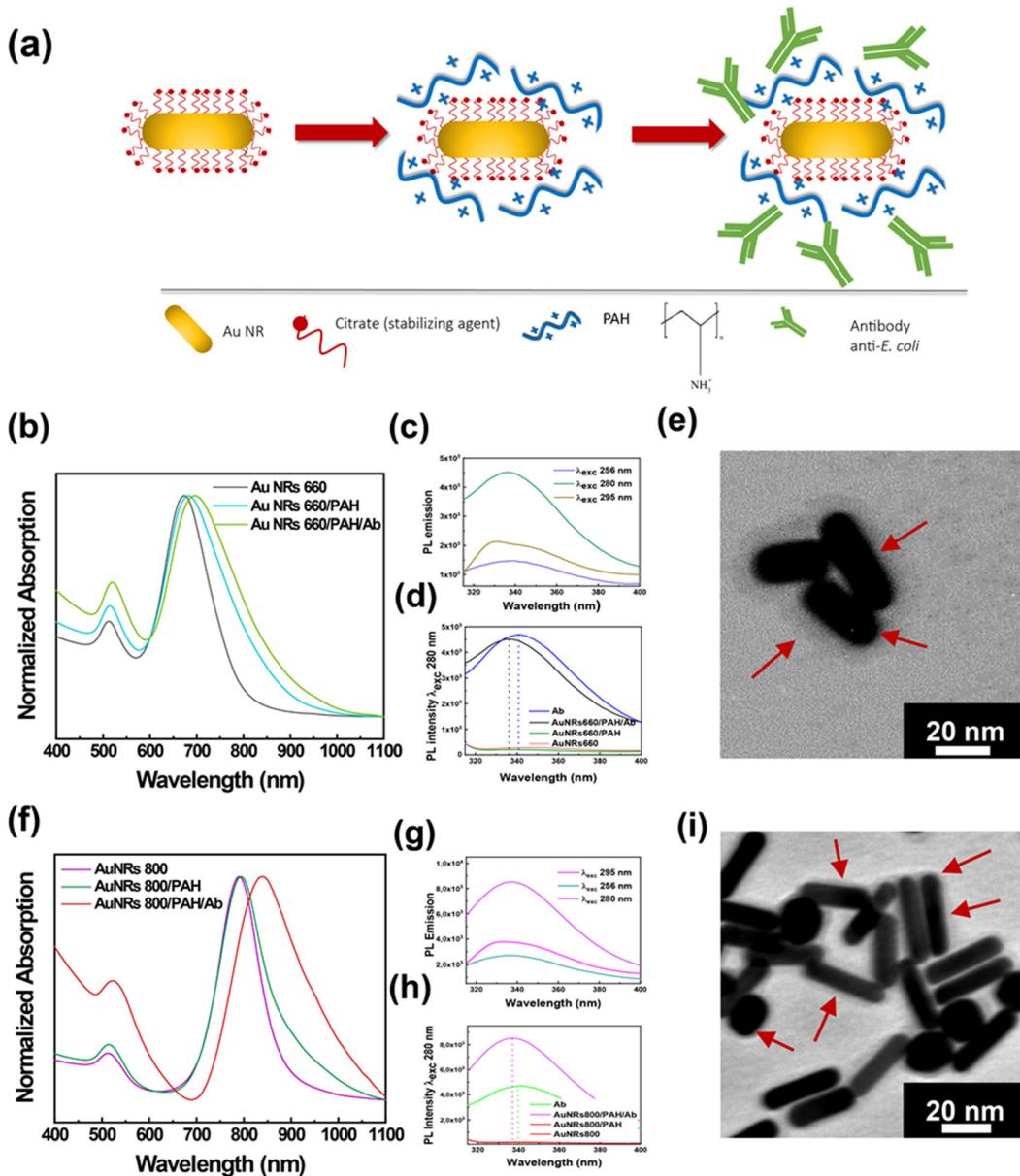
Fig. 1 Preparation and characterization of Au NR-based bioconjugates by the electrostatic linking method. Schematic of the experimental protocol adopted for Au NR bioconjugation with the Ab (a). Optical characterization of Au NR 660 Ab bioconjugate carried out by absorption (b) and photoluminescence spectroscopy (c and d). Transmission electron microscopy (TEM) analysis of the Au NR 660/PAH/Ab bioconjugate (e). Optical characterization of the Au NR 800 Ab bioconjugate, performed by absorption (f) and photoluminescence (g and h) spectroscopy. Transmission electron microscopy (TEM) analysis of the Au NR 800/PAH/Ab bioconjugate (i).

was incubated in a 10^3 CFU mL^{-1} E. coli dispersion (500 μL in minimum E) for 20 min. After this step, the photo-thermal disinfection experiment was performed by irradiating the sample with the 808 nm laser for two minutes at 29 W cm^{-2}. Subsequently, the sample was stained with propidium iodide (a staining agent used in many laboratories to identify dead cells by fluorescence microscopy and typically employed in kits such as the well-known LIVE/DEAD™ BacLight™ Bacterial Viability Kit) for further fluorescence microscopy and absorption spectroscopy characterization. In particular, 2 μL of propidium iodide dissolved in 500 μL of water was introduced to stain the substrate. The sample was left to incubate

for an additional 10 min in the dark and then rinsed with water for 1 min and dried under a nitrogen flow before measuring the absorption spectrum and performing the fluorescence microscopy analysis.

Finally, the substrate was washed three times with a 0.15 M NaCl solution (2 mL) to remove cells, rinsed with water, and dried under a nitrogen flow before collecting the absorption spectrum.

Contrast phase and fluorescence microscopy. Contrast phase and fluorescence microscopy images of active Au NR-based substrates were collected by using a ZEISS Axiolab 5 fluorescence microscope equipped with phase contrast

This journal is © The Royal Society of Chemistry 2022

Environ. Sci.: Nano, 2022, 9, 3343–3360 | 3347
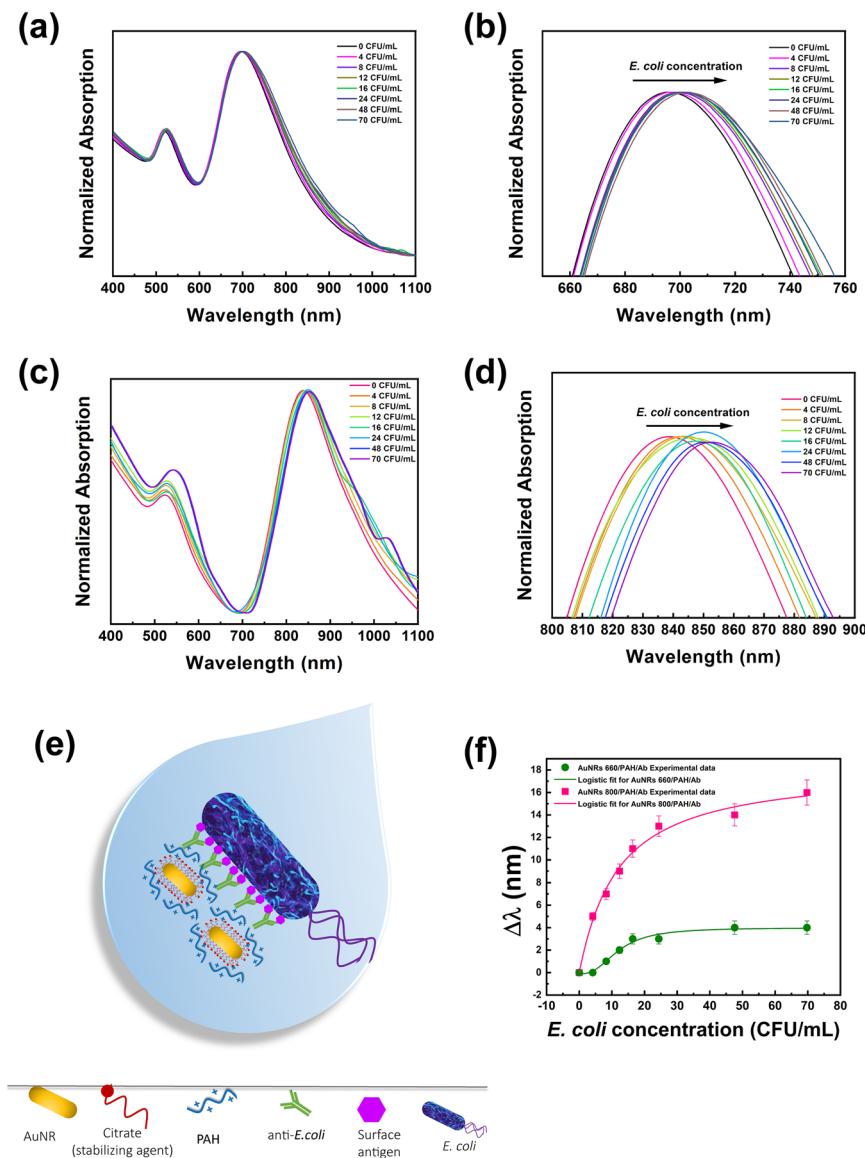
Fig. 2 Spectroscopic analysis of the ability of the Au NR-based bioconjugate to recognize *E. coli* cells in a water dispersion. Absorption spectra of the Au NR 660/PAH/Ab bioconjugate measured at different *E. coli* cell concentrations in the wavelength range from 400 nm to 1100 nm (a) and from 650 nm to 760 nm (b), highlighting the shift of the LSPRl position as a function of *E. coli* cell concentration. Absorption spectra of the Au NR 800/PAH/Ab bioconjugate measured at different *E. coli* cell concentrations in the wavelength range from 400 nm to 1100 nm (c) and from 800 nm to 900 nm (d), highlighting the shift of the LSPRl position as a function of *E. coli* cell amount. The absorption spectra are normalized to the intensity of the LSPRl to appreciate the spectroscopic features. The sketch (e) depicts the interaction between the bioconjugates and the *E. coli* cells mediated by the Ab. Comparison of the LSPRl shift (Δλ) measured for Au NR 660/PAH/Ab and Au NR 800/PAH/Ab as a function of the *E. coli* cell concentration in the water dispersion (f). The Δλ values were calculated considering the wavelength position of the LSPRl of each bioconjugate as a reference.

objectives and fluorescence modules. The morphological analysis was performed after the *E. coli* recognition tests to investigate the accumulation of *E. coli* cells promoted by the Ab functionalization.

Results and discussion

Selection of suitable Au NR dimensions for the biosensor fabrication

The first goal of the present work was to assess the ability of Au NR-based bioconjugates to produce a shift of the LSPRl when *E. coli* cells are recognized in a water dispersion. The results are crucial for selecting the optimal Au NR dimensions to fabricate substrates suitable for the spectroscopic detection of *E. coli* cells in water. To this end, Au NRs with different morphologies, namely Au NR 660 and Au NR 800, were functionalized with Abs to induce the unique antigen/antibody recognition, thus producing a local change of the *n* and a consequent optical shift of the LSPRl in the presence of *E. coli* cells.

Au NR-based bioconjugates were obtained using the electrostatic linking method.[26] This method simultaneously
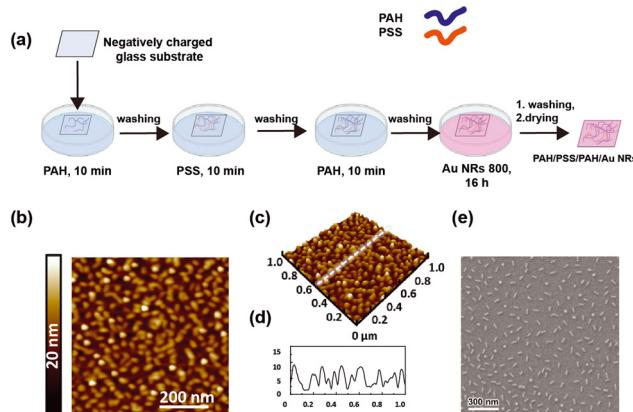
Fig. 3 Functionalization of glass substrates with Au NR 800. Schematic of the procedure used to modify a glass substrate with a polyelectrolyte multilayer (PEM) and incorporation of Au NR 800 by dipping (a). Topographical analysis of the Au NR 800-modified glass substrate by AFM (b) along with the corresponding three-dimensional topographic image (c) and the analysis of the line profile (d). Morphological characterization of a representative Au NR 800-functionalized substrate performed by SEM (e).

preserves two essential aspects for effective *n* sensing, *i.e.*, the unique spectroscopic properties of Au NRs and the structure of the Ab as a probe molecule.

In contrast with conventional physisorption-based approaches, the electrostatic linking method promotes the interactions between the nanostructure surface and the biomolecules by interposing one or more layers of PEs covering the NP surface.[26,27,37] Indeed, PEs provide a high density of charged groups accessible to polar functional groups of biomolecules to boost electrostatic attractions between the NP surface and the desired probe molecules.[26,37,38]

Although the electrostatic linking method provides limited control over Ab orientation at the NP surface,[37] it has been extensively exploited for therapeutic and sensing purposes.[32,38–40] Importantly, it can be regarded as a green approach for preparing bioconjugates because PEs are biocompatible functional materials,[41,42] allowing the circumvention of health and environmental hazardous chemicals such as 1-ethyl-3-(3-dimethylaminopropyl)carbodiimide. Moreover, the electrostatic linking method offers several degrees of freedom to optimize bioconjugation, which include pH, ionic strength, number of PE layers, and PE, Ab and NP concentrations.[27]

Fig. 1a shows a schematic representation of the experimental approach for achieving the bioconjugation of Au NRs with the Ab by the electrostatic linking method. Essentially, a two-step preparation protocol was used: in the first step, Au NRs were functionalized with PAH molecules resulting in the Au NR/PAH complex that, once isolated by centrifugation, was incubated for 30 min in the presence of the Ab to promote the electrostatic attractions between the PAH and the Ab. The resulting Au NR/PAH/Ab bioconjugate was collected by centrifugation, diluted in water, and characterized by spectroscopic and morphological techniques.
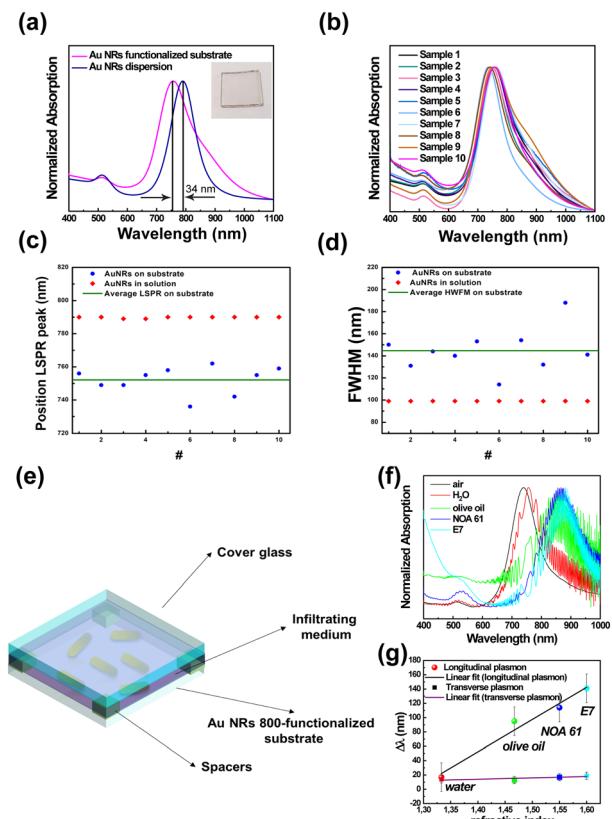
Fig. 4 Spectroscopic investigation on Au NR 800-functionalized substrates. (a) Absorption spectrum of a representative Au NR-functionalized substrate (magenta track) in comparison with the absorption spectrum of the corresponding colloidal dispersion (blue track). The inset shows a photographic picture of the Au NR 800-functionalized substrate. Spectroscopic characterization of ten Au NR 800-functionalized substrates to investigate the reproducibility of the preparation protocol (b). For each substrate the position of the LSPRl (c) and the FWHM value (d) are reported in comparison with the colloidal dispersion of Au NR 800. Schematic of the sample employed to measure the sensitivity to *n* by infiltrating the cell gap with different media (e). Absorption spectra of Au NR 800 cells infiltrated with different media that possess increasing *n* (f). Shift of the LSPRl and LSPRt, calculated with respect to the empty cell, as a function of the *n* of the infiltrating medium (g).

The surface functionalization of Au NR 660 with PAH molecules produced the Au NR 660/PAH complex, whose absorption spectroscopic profile is very close to that of the pristine Au NR 660. Indeed, as reported in Fig. 1b, Au NR 660 shows an absorption spectrum characterized by two typical plasmon bands of elongated NPs: the LSPRl centered at 673 nm and the LSPRt at 512 nm. After the functionalization step, the resulting Au NR 660/PAH complex exhibited a red-shift of the LSPRl of 10 nm. In contrast, the position of the LSPRt remained almost unchanged as it is less sensitive to local *n* variation.[13] Therefore, the 10 nm red-shift of the LSPRl band for the Au NR 660/PAH is associated with an increase of the local *n*,[13] indicating the generation of a PAH monolayer on the Au NR 660 surface. The assembly of such a monolayer can be promoted by electrostatic attractions between the negatively charged carboxylic groups of citrate molecules surrounding
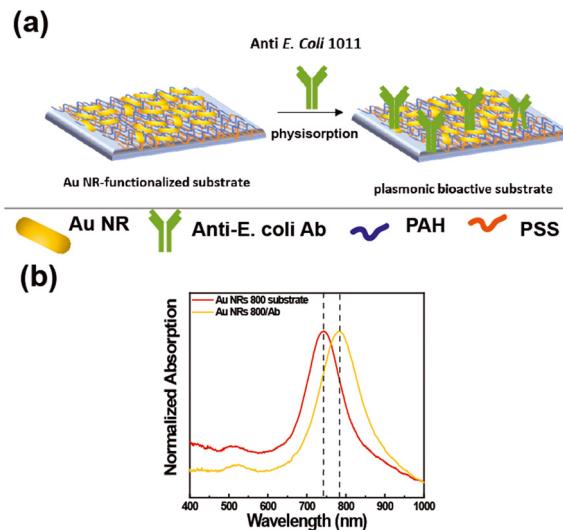
Fig. 5 Schematic of the procedure for bioactivating Au NR 800-functionalized substrates with the captured antibody able to recognize *E. coli* cells (a). Spectroscopic characterization of the bioactive plasmonic substrate after the incorporation of the Ab (yellow track) shows an optical red-shift of 40 nm with respect to the Au NR 800-functionalized substrate (b).

the surface of Au NR 660 and the positively charged amine groups of the PE. Moreover, the spectroscopic profile suggested that the Au NR 660/PAH preserved the colloidal stability and the monodispersity of pristine Au NR 660, considering that the spectroscopic fingerprints of pristine Au NR 660, namely LSPRl and LSPRt, in the gray track of Fig. 1b, are well defined in the absorption spectrum of the Au NR 660/PAH complex (cyan track in Fig. 1b).

The absorption spectrum of the Au NR 660/PAH/Ab bioconjugate (green track in Fig. 1b) pointed to a further shift of about 22 nm (with respect to Au NR 660) for the LSPRl. The red-shift of the LSPRl, in agreement with the Gans theory,[13] implies an alteration of the dielectric constant of the surrounding medium, clearly indicating the electrostatic accumulation of Ab molecules on the surface of the Au NR 660/PAH complex.

A photoluminescence (PL) spectroscopy investigation was carried out to assess whether, upon the bioconjugation by the electrostatic linking method, the Ab in the Au NR 660/PAH/Ab preserves its conformational stability and, therefore, its biological functions to recognize antigens on the *E. coli* cell's surface are preserved.

In particular, this investigation was performed by exciting the amino acid residues with intrinsic fluorescence, namely, phenylalanine (Phe), tyrosine (Tyr), and tryptophan (Trp), whose PL spectrum is sensitive to alterations of the secondary and tertiary structure, especially for Trp.[43] The characterization of the Au NR 660/PAH/Ab bioconjugate by PL spectroscopy is shown in Fig. 1c and d. Fig. 1c shows the PL spectra of the Au NR 660/PAH/Ab collected by exciting the bioconjugate at 256 nm to analyze the emission from Phe, at 280 nm to evaluate the emission from Tyr and Trp, and at 295 nm to

selectively measure the emission from Trp. The PL spectra clearly show the typical emission signals associated with Phe, Tyr, and Trp residues. In particular, by exciting the sample at 280 nm, an intense and broad emission band associated with Tyr and Trp appeared. The photoluminescence spectra in Fig. 1d were collected by selectively exciting the Tyr and Trp residues, both for the Au NR 660/PAH/Ab (black track) and for the free Ab (blue track), respectively. By exciting the Au NR 660/PAH/Ab bioconjugate at 280 nm, a blue shift of the emission, from 341 nm (for the free Ab) to 336 nm (for the Au NR 660/PAH/Ab bioconjugate) was measured (Fig. 1d). The observed blue shift indicates that the Tyr and Trp groups within the Au NR 660/PAH/Ab bioconjugate are less exposed to the solvent than the Tyr and Trp residues in the free Ab.[43] Accordingly, Tyr and Trp residues may play a relevant role in achieving the electrostatic binding between Au NR 660/PAH and the Ab. We can infer that Tyr and Trp residues can promote electrostatic attractions involving the positively charged PAH amine groups and the hydroxyl groups carried on the benzene ring of Tyr as well as π-interactions involving the aromatic rings of Tyr and Trp.

The morphological analysis of the bioconjugate Au NR 660/PAH/Ab, carried out by TEM, is reported in Fig. 1e. The Au NR 660/PAH/Ab bioconjugate (Fig. 1e) is characterized by an outer surface layer (5–7 nm) with higher contrast to the micrograph background. The formation of the "corona layer" highlighted in Fig. 1e has been very often reported in the literature as proof of an effective NP surface functionalization with high molecular weight compounds,[44,45] thus indicating the formation of an antibody layer on the Au NR 660/PAH NPs' surface.

The spectroscopic and morphologic characterization of the Au NR 800/PAH/Ab bioconjugate is reported in Fig. 1f. The wrapping with the PAH layer shifted the position of the LSPRl of Au NR 800 from 790 nm (Fig. 1f, magenta track) to 794 nm (Fig. 1f, green track). After the bioconjugation process occurred, the LSPRl was centered at 838 nm, with an overall red-shift of 48 nm (Fig. 1f, red track). Such a plasmonic red-shift, more intense than the one obtained for the Au NR 660/PAH/Ab bioconjugate (22 nm), accounts for the higher sensitivity to *n* changes, confirming the strong correlation between the aspect ratio of Au NRs and their *n* sensitivity.[13]

Moreover, in the red track of Fig. 1f, the increase of the absorption intensity at lower wavelengths can be associated with the presence of the Ab molecules linked to the Au NR 800/PAH surface.[16]

The analysis of the conformational stability of the Ab in the Au NR 800/PAH/Ab bioconjugate, carried out by PL spectroscopy, is shown in Fig. 1g and h. On exciting the bioconjugate at 256 nm, 280 nm, and 295 nm, the emission bands of Phe, Tyr/Trp, and Trp, respectively, were detected (Fig. 1g). The PL spectra in Fig. 1h were collected by selectively exciting the Tyr and Trp residues, both for the Au NR 800/PAH/Ab and the free Ab.

3350 | *Environ. Sci.: Nano*, 2022, **9**, 3343–3360

This journal is © The Royal Society of Chemistry 2022
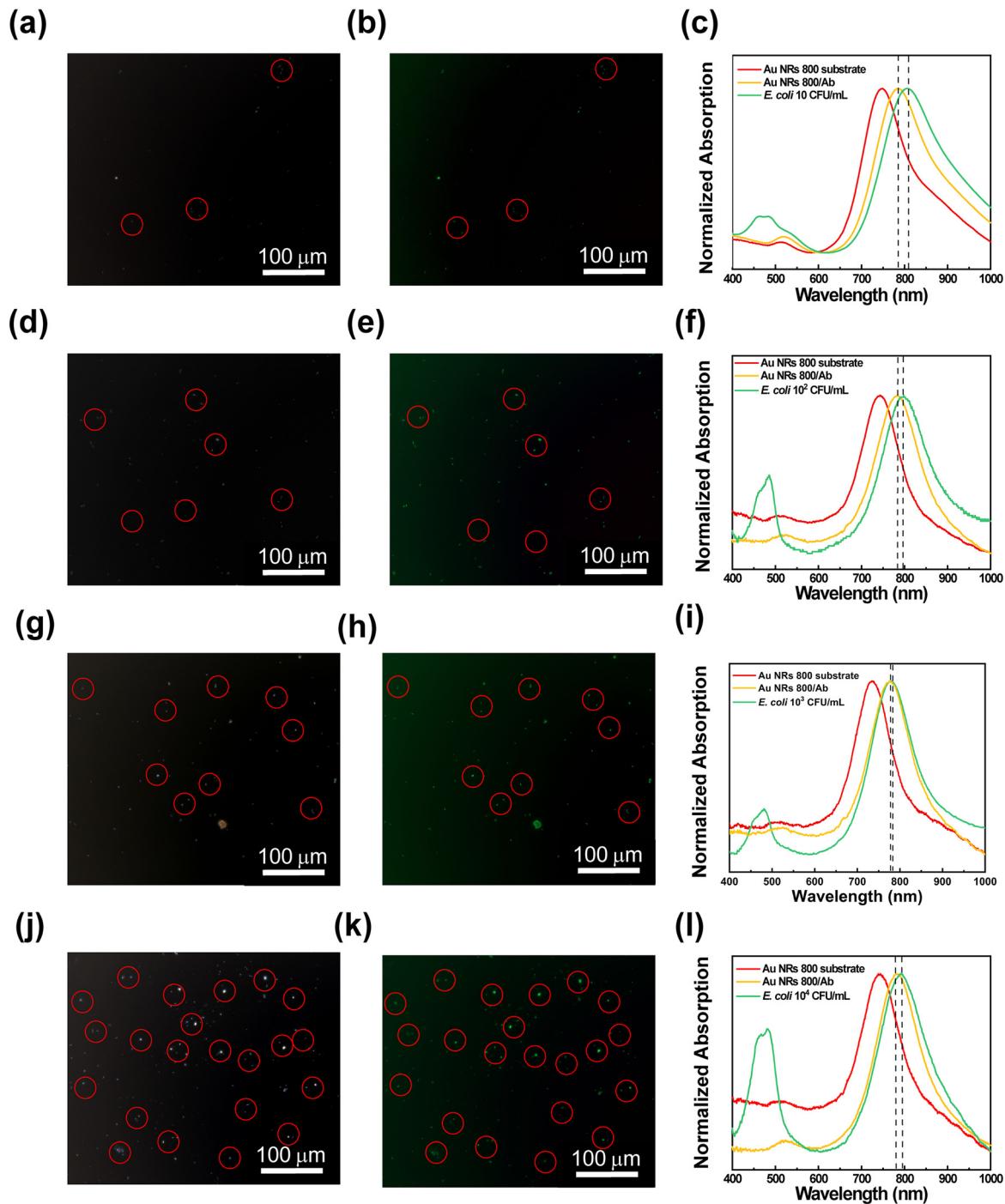
Fig. 6 Characterization of the bioactive plasmonic substrates after incubating *E. coli* dispersions in minimum E at different cell concentrations. Contrast phase microscopy images (a, d, g and j), fluorescence microscopy images (b, e, h and k), and absorption spectroscopy characterization (c, f, i and l) of the bioactive plasmonic substrate progressively incubated in a 10, 10^2, 10^3, and 10^4 CFU mL^{-1} *E. coli* cell dispersion.

Experimental results point out that the emission peak position moved from 340 nm (for the free Ab) to 337 nm for Au NR 800/PAH/Ab. Likewise, for the Au NR 660/PAH/Ab, such a result indicates that the binding between the Au NR 800/PAH and the Ab could involve the hydroxyl groups carried on Tyr and aromatic moieties of Tyr and Trp that induce π-interactions. The TEM analysis of the Au NR 800/PAH/Ab bioconjugate reported in Fig. 1i highlighted the occurrence of high aspect ratio Au NRs. Moreover, also Au NR 800/PAH/Ab bioconjugates are characterized by a "corona layer" associated with the presence of the Ab assembled on the Au NR 800/PAH surface, as previously reported for Au NR 660/PAH/Ab.

The characterization techniques demonstrated the electrostatic linking method's effectiveness in producing Au NR-based bioconjugates with properties suitable for LSPR biosensing applications in terms of spectroscopic, colloidal, and structural features. Accordingly, a simple assay in a water dispersion was carried out to assess the LSPR biosensing properties of the Au NR-based bioconjugates. In particular, the assay examined the ability of the bioconjugates to produce spectroscopic response upon recognition of *E. coli* cells.

After the preparation step, the dispersions of both the bioconjugates were suitably diluted to achieve the same absorption intensity for the LSPRl (0.5 absorption units). After that, aliquots of *E. coli* cells from a 10^3 CFU mL^{-1} water dispersion were sequentially added to the bioconjugate dispersions. The absorption spectrum was collected after keeping the mixture under vigorous stirring for 10 min. The total volume of *E. coli* cells produced a 10% increase of the total volume of the dispersion, resulting in a minor experimental error on the concentration of the bioconjugate at the end of the experiment.

Experimental results reported in Fig. 2a depict that both LSPRt and LSPRl of Au NR 660/PAH/Ab are detectable regardless of the *E. coli* cell concentration. The concentration range of *E. coli* examined in this assay (from 4 to 70 CFU mL^{-1}) did not produce Au NR aggregation, as the presence of aggregates would cause a broadening and a significant shift (greater than 200 nm (ref. 46)) of the plasmon bands. Fig. 2b highlights how the LSPRl of the Au NR 660/PAH/Ab is progressively red-shifted as the concentration of *E. coli* cells increased from 1 nm at 8 CFU mL^{-1} to 4 nm at 70 CFU mL^{-1}. Fig. 2c clearly shows that also Au NR 800/PAH/Ab maintains unaltered its spectroscopic features (for both LSPRt and LSPRl bands) despite the progressive increase of the *E. coli* concentration. However, it is worth noting the occurrence (Fig. 2d) of an evident and gradual red-shift of the LSPRl of Au NR 800/PAH/Ab in the range from 5 nm (at 4 CFU mL^{-1}) to 16 nm (at 70 CFU mL^{-1}).

The LSPRl position is considered a sensing parameter because this plasmonic mode is more sensitive to *n* variations.[15] Fig. 2b–d highlight that the progressive increase of *E. coli* cell concentration produces a shift of the corresponding LSPRl band towards higher wavelength values for both the bioconjugates. This behavior is associated with the gradual increase of the surrounding *n*, associated with the gradual increase of *E. coli* cell amount, induced by the presence of the Ab on the Au NR.

The Ab loaded on the Au NR surface effectively promotes the accumulation of Au NR-based bioconjugates on the bacterial surface through the univocal and selective antigen–Ab recognition, as sketched in Fig. 2e.

Still, instead, it is preferentially promoted by the univocal antigen/antibody recognition occurring on the proximity of the Au NR surface. According to the reported experimental data in Fig. 2a–d, the spectroscopic behaviour of both Au NR 660/PAH/Ab and Au NR 800/PAH/Ab in the presence of *E. coli* cells highlighted the ability of the bioconjugates to recognize *E. coli* cells and produce a spectroscopic response consistent

with the bacterial concentration. As demonstrated by experimental data, the measured red-shift is proportional to the bacterial loading, as shown by similar studies.[23,46]

The plot in Fig. 2f aims at comparing the sensing performance of the Au NR 660/PAH/Ab and Au NR 800/PAH/Ab bioconjugates by reporting the respective $\Delta\lambda$ (defined as the optical shift of the LSPRl of each bioconjugate after the stepwise introduction of an *E. coli* aliquot) as a function of the *E. coli* cell concentration.

Although both the bioconjugates were able to produce a spectroscopic response concomitant with the increase of *E. coli* cell amount, Fig. 2f highlights a superior sensing performance of Au NR 800/PAH/Ab to that of Au NR 660/PAH/Ab.

As such, in all the investigated concentration ranges, the $\Delta\lambda$ values produced by Au NR 800/PAH/Ab were higher than the ones measured for Au NR 660/PAH/Ab.

As an example, an *E. coli* loading of 16 CFU mL^{-1} determined a $\Delta\lambda$ of 11 nm for Au NR 800/PAH/Ab and a $\Delta\lambda$ of 3 nm for Au NR 660/PAH/Ab. Moreover, the Au NR 800/PAH/Ab bioconjugate was able to detect also a lower concentration of *E. coli* cells. Indeed, a concentration of 4 CFU mL^{-1} did not affect the position of the LSPRl of Au NR 660/PAH/Ab but shifted with a $\Delta\lambda$ of 5 nm the LSPRl of the Au NR 800/PAH/Ab bioconjugate. Both the curves of $\Delta\lambda$ values as a function of *E. coli* concentration showed an initial increase of $\Delta\lambda$, followed by a plateau for *E. coli* concentration values above 24 CFU mL^{-1}. To better investigate the sensing ability of the bioconjugates Au NR 660/PAH/Ab and Au NR 800/PAH/Ab, the experimental points of Fig. 2f were interpolated using a four-parameter logistic equation[47,48] from the software OriginPro 2020 (logistic fit function), resulting in eqn (1).

$$\Delta\lambda = \Delta\lambda_{\max} + \frac{\Delta\lambda_0 - \Delta\lambda_{\max}}{1 + \left(\frac{x}{c}\right)^p} \qquad (1)$$

The interpolation (see eqn (1) and Table S1 of the ESI†) provides a solid and robust interpretation of the interaction between *E. coli* cells (that is here regarded/interpreted as a macromolecule) and bioconjugates (ligand) in terms of affinity, where $\Delta\lambda_{\max}$ corresponds to the maximum value of the optical shift, $\Delta\lambda_0$ is the minimum optical shift that the bioconjugate can provide, x is the *E. coli* cell concentration, p indicates the degree of cooperativity, and c is the constant that provides the cell concentration at which half of $\Delta\lambda$ is achieved.[49] Therefore, the lower the c value, the higher the affinity between the *E. coli* cells and the bioconjugate. Hence, according to the sigmoidal fitting, c values are 12 ± 2 CFU mL^{-1} and 11 ± 5 CFU mL^{-1} for the Au NR 660/PAH/Ab and Au NR 800/PAH/Ab bioconjugates, respectively. This small difference suggested that both the Au NR 660/PAH/Ab and the Au NR 800/PAH/Ab bioconjugates exhibit a good affinity towards *E. coli* cell surface antigens.

Furthermore, the p value calculated for the assay carried out in the presence of Au NR 660/PAH/Ab is 2.56 ± 0.64, while the p value obtained from the interpolation of the results from Au NR 800/PAH/Ab is 1.04 ± 0.21. This difference

indicates a progressive decrease in the affinity between the bioconjugate and the *E. coli* antigens with the increase of the cell concentration. Such a negatively cooperating binding appeared less intense for the Au NR 800/PAH/Ab bioconjugate. Moreover, it was possible to estimate a LOD (corresponding to the IC_{10} value calculated from the four-parameter logistic curve fit)[48] of 5.07 CFU mL^{-1} for Au NR 660/PAH/Ab and a LOD of 1.4 CFU mL^{-1} for Au NR 800/PAH/Ab. The ensemble of the experimental results pointed out the superior sensing performance of the Au NR 800/PAH/Ab bioconjugate to that of the Au NR 660/PAH/Ab bioconjugate under the investigated experimental conditions. Indeed, based on interpolation results, for the same *E. coli* cell concentration, the Au NR 800/PAH/Ab bioconjugate produced higher values of $\Delta\lambda$. Accordingly, Au NR 800 NPs were selected as plasmonic NPs to fabricate an LSPR biosensor on rigid substrates.

Fabrication and characterization of Au NR 800-functionalized substrates

Inspired by the optimal LSPR biosensing performance achieved for the colloidal dispersion of the Au NR 800/PAH/Ab bioconjugate, the realization of an array of Au NR 800 on the glass substrate was carried out to obtain optimal morphological properties such as high surface coverage, suitable interparticle spacing, even Au NR distribution, and no presence of Au NR aggregates.[50]

The electrostatic layer-by-layer (LbL) assembly technique was here employed as a suitable and well-established fabrication approach to obtain the desired morphological and optical features.[32,51–53]

As shown in Fig. 3a, the modification of the glass substrate was realized by depositing a PE multilayer with the sequence PAH/PSS/PAH.

The sequential alternation of a weak positively charged PE (PAH) and a strong negatively charged PE (PSS) minimizes PE interdiffusion and provides a more uniform surface charge density that cannot be obtained from utilizing a monolayer.[54,55] An even distribution of surface charges results in uniform distribution of the Au NR 800, promoted by the electrostatic attractions between PAH and the carboxylic groups exposed on the Au NR surface. Moreover, previous investigations demonstrated that PAH, having a chemical structure characterized by a linear backbone, can facilitate the generation of a uniform Au NR layer of isolated NPs, thus obtaining the features of a monodisperse colloidal dispersion on a solid support.[32,56]

After building the PE multilayer, the incorporation of Au NR 800 was realized by immersing the PE-modified glass substrate in an Au NR colloidal dispersion for 16 h, thus achieving a homogeneous substrate with a uniform pink tone, indicating the loading of Au NRs (inset of Fig. 4a).

The morphological characterization performed by atomic force microscopy (AFM) (Fig. 3b–d) and SEM (Fig. 3e) depicts the presence of a uniform Au NR 800 layer over a large area (1 cm^2). Indeed, the topographic investigation shows asperi-

ties of anisotropic shape, with an even distribution over the investigated area of 1 μm × 1 μm. Interestingly, the analysis of the height profile results in an average value of 10 nm (Fig. 3d), in agreement with the dimension of the short side of Au NR 800 measured by TEM (Fig. 1f).

Such a result supports the occurrence of an Au NR monolayer on the substrate. It is strongly consistent with the SEM analysis (Fig. 3f) reporting the presence of individual Au NRs separated from each other and the absence of aggregates. The statistical analysis performed on SEM micrographs reveals that the Au NR 800 on substrates possess a fill fraction of 5.9% ± 0.2% along with an interparticle distance of 142 ± 50 nm and a density of about 215 Au NRs per μm^2.

As reported in Fig. 4a (magenta track), the spectral analysis of the realized sample clearly shows two spectroscopic fingerprints of Au NRs, *i.e.*, the LSPRt centered at 514 nm and the LSPRl centered at 756 nm. The LSPRl of the Au NR 800-functionalized substrate is 34 nm blue-shifted to the Au NR 800 colloidal dispersion, in agreement with previously reported results.[56,57] In addition, the observed blue-shift is promoted by the change (decrease) of the n of the chemical medium surrounding[13] the Au NR 800 that changed from water ($n = 1.33$) to air ($n = 1$).[20]

It is noteworthy that the spectral response of the Au NR 800-functionalized substrate (Fig. 4a, magenta curve) did not show any visible absorption signal in the long NIR range, suggesting that due to relatively long distances among the immobilized nano-objects, the multipolar couplings among surface plasmon resonances are minimized.[56,58]

The absorption spectra of ten different Au NR-modified glass samples (Fig. 4b), fabricated by reproducing the same protocol, demonstrated the repeatability of the fabrication process.

As shown in Fig. 4b, the ten spectral profiles almost overlap; moreover, the LSPRl position is distributed around the mean value of 752 nm ± 8 nm (Fig. 4c), while according to experimental data reported in Fig. 4d, the mean value of the FWHM is 145 ± 18 nm. The two standard deviation values suggested that the adopted protocol is suitable for the large-scale production of Au NR-modified glass substrates with excellent reproducibility.

Using Au NR 800-functionalized substrates as rigid platforms, we fabricated glass cells (Fig. 4e) that were subsequently infiltrated with several media possessing different n (Table S2 in ESI†) to quantify, by absorption spectroscopy, the n bulk sensitivity of randomly immobilized Au NR 800.

The absorption spectra reported in Fig. 4f, beyond showing the interference fringes[59] accounting for the micrometer size gap between the Au NR 800 substrate and the glass cover, point out a gradual red-shift ($\Delta\lambda$) of both LSPRt and LSPRl of Au NRs with the increase of the n of the infiltrating medium.

The resulting $\Delta\lambda$ measured at the plasmon band positions of the empty cells are reported as a function of n values in Fig. 4f. Following theoretical predictions focusing on colloidal dispersions of Au NRs, experimental results highlight a

This journal is © The Royal Society of Chemistry 2022

Environ. Sci.: Nano, 2022, **9**, 3343–3360 | **3353**

linear correlation between the n of the infiltrating medium and the $\Delta\lambda$ (ref. 14) on a rigid substrate. In particular, a bulk sensitivity (S)[60] of 456 nm per refractive index unit (RIU) and a figure of merit (evaluated as S/FWHM)[60] of 3.1 were calculated for the LSPRl.

The morphological and optical investigation of Au NR 800-functionalized substrates and a stability test reported in Fig. SI3† highlighted that the immobilization approach was suitable for achieving the desired properties as an LSPR-based biosensor.

Indeed, the topographic, morphological, and optical investigation pointed out the occurrence of a uniform layer of a Au NR 800 array. In this array, Au NR 800 appeared as individual nano-objects, and hence their exposed surface available for interaction with the biorecognition element and the analyte is maximized, resulting in high-quality sensing performance.[28,29] Indeed, the S value refereed to the LSPRl was calculated to be higher than previously reported results for analogous plasmonic-based platforms.[21,57,61]

Fabrication and characterization of biologically active Au NR-functionalized substrates

The extraordinary sensing capabilities of Au NR 800-functionalized substrates were considered extremely promising for the fabrication of a label-free LSPR biosensor for biomolecule recognition. To this end, the Au NR 800-functionalized substrates were employed as plasmonic platforms for generating biologically active plasmonic substrates, realized by incorporating the above-explored Ab as a trapping antibody and biorecognition element (Fig. 5).

The Ab promotes the confinement of $E.\ coli$ cells on the Au NR 800 array through the univocal antigen–antibody recognition that alters the n experienced by the immobilized Au NR 800. As a result, the recognition mechanism triggers a plasmonic-based color change, similar to the previously demonstrated water dispersions (Fig. 2).

Fig. 5a shows a schematic of the incorporation of the Ab on the Au NR 800 array. However, the Ab's incorporation can also be promoted by the electrostatic interactions between the PAH layer underlying Au NRs, which covers about 94% of the surface, and the negatively charged functional groups of the Ab. The absorption spectra (Fig. 5b) point out a 40 nm red-shift of the LSPRl of the substrate following the Ab physisorption step, thus indicating the accomplishment of Ab incorporation.

The ability of the resulting substrates to attract and recognize $E.\ coli$ cells at different concentration levels was investigated by performing microscopy and spectroscopy analysis. To this end, the bioactive substrates were incubated for 30 min in $E.\ coli$ dispersions at several concentrations ranging from 10 CFU mL^{-1} to 10^4 CFU mL^{-1}, washed, dried, and finally characterized. Experimental data from substrate characterization are reported in Fig. 6, showing, for each bioactive substrate, the contrast phase images, the corresponding fluorescence microscopy images, and the absorption spectroscopy investigation.

The contrast phase images in Fig. 6(a, d, g, and j) display bright spots (red circles) of elongated shape, showing an average length of 1.9 ± 0.2 μm that can be associated with $E.\ coli$ cells accumulated on the bioactive substrates. The corresponding fluorescence microscopy images in Fig. 6(b, e, h, and k) highlight the presence of progressively increasing green spots (red circles) uniformly distributed on the surface of the biofunctionalized plasmonic substrates. They are associated with $E.\ coli$ cells stained by the SYTO 9™ fluorescent dye. The number of the $E.\ coli$ cells captured by each substrate, according to the scheme reported in Fig. 7a, was estimated from fluorescence microscopy images (using ImageJ microscopy software) by counting cells in a region of interest of 90 000 μm^2. As a result, despite the washing procedure, the number of $E.\ coli$ cells deposited on each bioactive plasmonic substrate increased with the increase of $E.\ coli$ cell concentration in the respective dispersion (as reported in Fig. SI4†), thus demonstrating the ability of the bioactive substrates to capture $E.\ coli$ cells and to accumulate several bacteria proportional to the utilized $E.\ coli$ cell concentration (Fig. SI4†). In contrast, only a few green spots were observed for the Au NR 800 substrate without bioactivation, as reported in the control experiments (Fig. SI5b†). Subsequently, to assess whether the accumulation of $E.\ coli$ cells can also produce a spectroscopic response, the absorption spectra of the active Au NR 800-modified substrates were collected and reported in Fig. 6c, f, i, and l. They show the absorption spectra of:

1. The Au NR 800-functionalized glass substrate (red tracks).

2. The bioactive substrates after incorporating the Ab (yellow tracks).
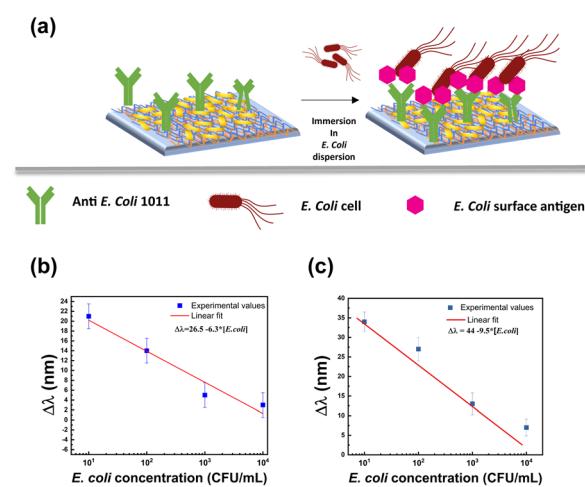
Fig. 7 Schematic of the mechanism of capturing $E.\ coli$ cells promoted by the Ab incorporated on the plasmonic substrate. (a) Optical shift ($\Delta\lambda$) as a function of $E.\ coli$ concentration in the incubation dispersion, reported on a logarithmic scale for $E.\ coli$ recognition experiments in the presence of SYTO 9™ (b) and in the absence of SYTO 9™ (c).

3. The bioactive substrates after the incubation in *E. coli* dispersions at different bacterial concentrations (green tracks).

The green curves (Fig. 6c, f, i, and l) exhibit an absorption signal between 400 nm and 500 nm, associated with SYTO 9™ molecules that bind to *E. coli* DNA. It is noteworthy that the LSPRl of each Au NRs800/Ab substrate shifted toward higher wavelengths following the incubation in the *E. coli* dispersion. In particular, the 10 CFU mL^{-1} dispersion resulted in a red-shift of 21 nm, while 10^2 CFU mL^{-1}, 10^3 CFU mL^{-1}, and 10^4 CFU mL^{-1} dispersions produced a red-shift of 14 nm, 5 nm, and 3 nm, respectively.

Hence, the sensitivity of Au NR 800/Ab decreases as the *E. coli* concentration increases. To explain this behaviour, different from the results illustrated in Fig. 2f, it is worth considering the complexity of the phenomena occurring at the solid/liquid interfaces.

Under the investigated experimental conditions, the *E. coli* cells accumulate on the Au NR 800/Ab substrates by a diffusion-driven process. Due to the biofunctionalization, the cells progressively layer Au NR 800/Ab substrates in an amount proportional to the cells' concentration for each dispersion (see Fig. SI4†). As a consequence of the increase in the thickness of the material, over-layering the array of Au NRs produced a decrease in electric field intensity that reduces LSPR sensitivity occurring at higher *E. coli* concentrations.[62,63]

Indeed, the sensitivity of Au NR arrays is affected by the distance from the Au NR surface.[64,65] Moreover, the *E. coli* cells progressively occupy the Au NR 800/Ab surface sites available for antigen–Ab recognition, thus reducing the sensitivity as the *E. coli* concentration increases, accounting for the decrease of $\Delta\lambda$ values.

Furthermore, by plotting the resulting $\Delta\lambda$ values as a function of the *E. coli* cell concentration (Fig. 7b), it was possible to determine a linear correlation that allowed us to estimate a LOD[33,34] of 8.4 CFU mL^{-1}.

Notably, the decrease in sensitivity with the increase of the *E. coli* concentration was also evidenced in control experiments performed without STYO 9™ molecules. Experimental results reported in Fig. SI6† highlighted the efficiency of the bioactive substrates to respond even at very low CFU mL^{-1}.

For instance, the immersion in the 10 CFU mL^{-1} *E. coli* dispersion produced a $\Delta\lambda$ of 34 nm (Fig. SI6a†). Moreover, the linear fit resulting from plotting the $\Delta\lambda$ as a function of *E. coli* concentration allowed us to estimate a LOD of 8.7 CFU mL^{-1} and a sensitivity[66] of 9.5 nm mL CFU^{-1} (Fig. 7c).

Further control experiments were performed to clarify the effect of SYTO 9™ molecules, which plays the twofold role of (i) demonstrating that the spectroscopic shifts are a consequence of a biorecognition event and (ii) enabling a cross-check on the presence of *E. coli* on the Au NRs/800 Ab substrate.

Experimental results reported in Fig. SI7a and b† demonstrated that in the absence of *E. coli* cells, the SYTO 9™ molecules determined a red-shift of the LSPRl. Moreover, the com-

parison between the data reported in Fig. 7b and c indicated that the SYTO 9™ molecules show the drawback of behaving as a passivation layer, thus limiting the sensitivity of the bioactive substrates.

It is noteworthy that the proposed LSPR biosensor displayed higher values of the LSPRl shifts for the lower concentration of bacteria. The Au NR 800/Ab-based biosensor even demonstrated a 1.5 times higher sensitivity in the absence of the fluorescent dye, thus revealing a highly efficient label-free nanoplatform for detecting *E. coli* at low concentrations. Remarkably, it showed a LOD lower than that of previously reported LSPR biosensors based on immobilized plasmonic NPs.[18–20]

In addition, we performed a specificity experiment by testing the optical response of the Au NR 800/Ab substrates in the presence of another coliform: the *Salmonella enterica* serovar *Typhimurium* LT2. Experimental results reported in Fig. SI8† demonstrate that the *S. Thyphimurium* did not alter the LSPRl position of Au NR 800/Ab, thus providing conclusive evidence of the high specificity of the biofunctionalized Au NR 800/Ab substrates.

Reusable biosensor *via* multicolor thermoplasmonic disinfection

To investigate the possibility of reutilizing the proposed biosensor, we have studied a photo-thermal-based disinfection process by exploiting the thermoplasmonic properties of Au NRs.

The photothermal performance of the functionalized substrates was investigated with a two-color optical setup, as described in Fig. 8a.

It allows the investigation of the thermoplasmonic properties using a CW laser beam emitting at 532 nm (green laser) and 808 nm (NIR laser) that selectively excite LSPRt and LSPRl modes, respectively.

The two-color optical setup allows mimicking a solar-light disinfection process or better said a broadband photothermal disinfection process. The light-to-heat conversion efficiency was measured by a thermal camera that provides thermographic images that are reported in Fig. 8b and c for the green and the NIR laser, respectively.

From the analysis of thermographic images collected during the irradiation time, a plot reporting the maximum temperature increase (ΔT_{max}) as a function of irradiation time was obtained (time–temperature profiles), as shown in Fig. 8d and e.

In particular, the time–temperature profiles were collected at different light intensities (power densities) in the range from 4.3 W cm^{-2} to 25.7 W cm^{-2} for the green laser (Fig. 8d) and from 5 W cm^{-2} to 29 W cm^{-2} for the NIR laser (Fig. 8e). Fig. 8d and e show that under laser irradiation, irrespective of the light intensity, the samples promoted a progressive temperature increase for 2 min followed by gradual cooling, which occurred when the laser sources were turned off.

This journal is © The Royal Society of Chemistry 2022

Environ. Sci.: Nano, 2022, **9**, 3343–3360 | **3355**
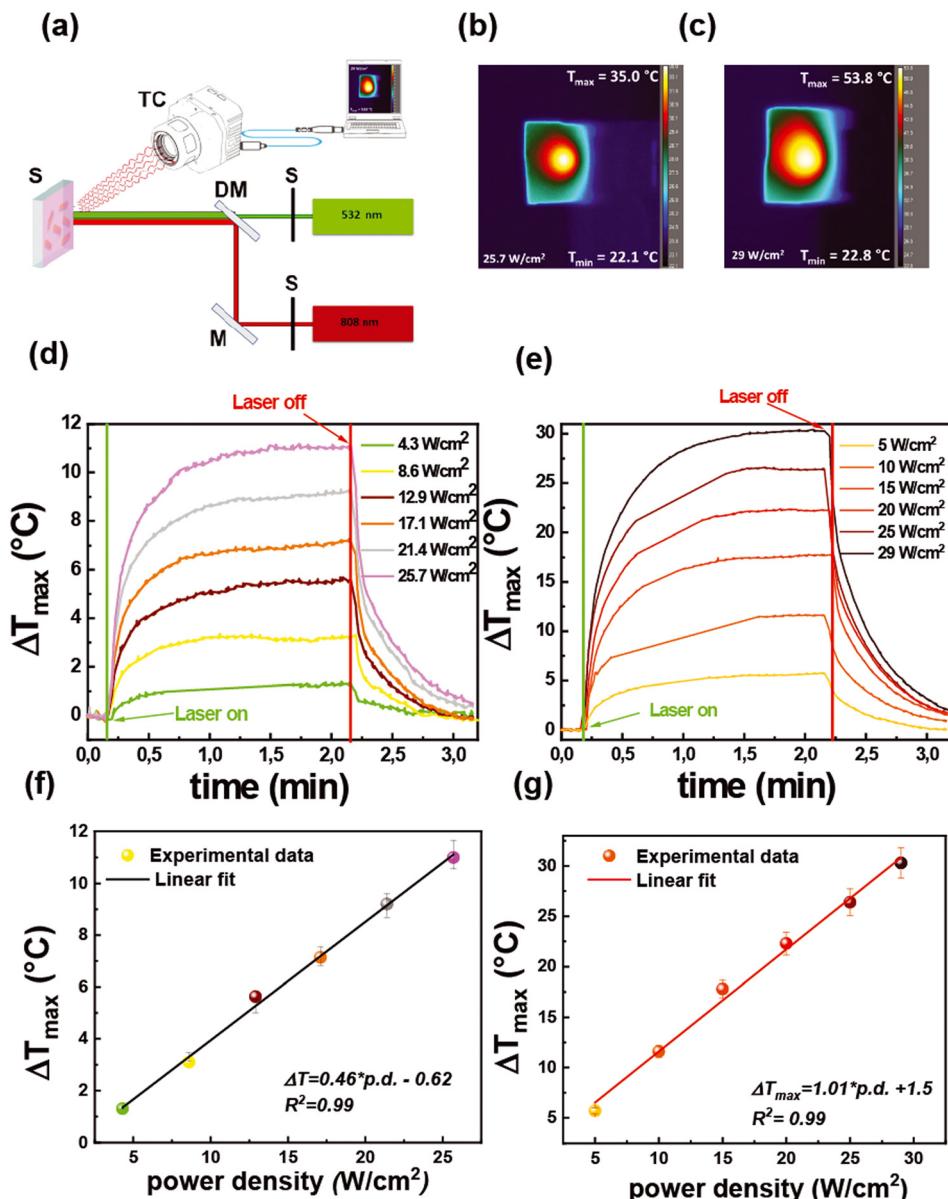
Fig. 8 Photothermal investigation on Au NR 800-functionalized substrates performed under pump beam illumination at 532 nm and 808 nm. (a) Schematic of the experimental setup designed to analyse the photothermal properties of the Au NR 800-functionalized substrates: the thermo-optical setup is designed so that the laser spot is focused on the centre of the substrate, which is monitored with a thermal camera to record the thermoplasmonic heating upon laser illumination. Thermographic images were collected at the end of the irradiation time performed with the laser source emitting at 532 nm (b) and 808 nm (c). The thermographic images are referred to the experiment conducted with a laser power density of 25.7 W cm^{-2} for the laser emitting at 532 nm and with the power density of 29 W cm^{-2} nm^{-1} for the laser emitting at 808 nm. Temperature increase (ΔT) as a function of irradiation time at different values of laser power density obtained with the laser source emitting at 532 nm (d) and 808 nm (e). Linear fit of the maximum temperature variations (ΔT_{max}) as a function of the intensity of the pump beam for the laser source emitting at 532 nm (f) and 808 nm (g).

For both the light sources, as shown in Fig. 8f and g, the ΔT_{max} values increased linearly with the power intensity of the laser beam, in agreement with theoretical models.[67] Notably, at a comparable power density, a different value of ΔT_{max} was achieved according to the laser source. Indeed, the irradiation with the green laser with a power density of 12.9 W cm^{-2} produced a ΔT_{max} of 5.6 °C, while setting the NIR laser at a similar intensity value (10 W cm^{-2}) gave a ΔT_{max} of 11.6 °C. On increasing the light intensity of the green laser at 25.7

W cm^{-2}, the ΔT_{max} rose at 11.1 °C, while at the intensity of 25 W cm^{-2}, the 2 min irradiation with the NIR laser generated a ΔT_{max} of 30.3 °C. Such results accounted for the higher photo-thermal efficiency of the LSPRl (excited with the NIR laser) than that of the LSPRt (excited with the green laser).

The excellent ability of Au NR 800 substrates to behave as photothermal transducers[68] is here highly advantageous considering that under the investigated experimental parameters it was possible to achieve with the NIR laser at 29 W cm^{-2} a

3356 | *Environ. Sci.: Nano*, 2022, **9**, 3343–3360

This journal is © The Royal Society of Chemistry 2022

(a)
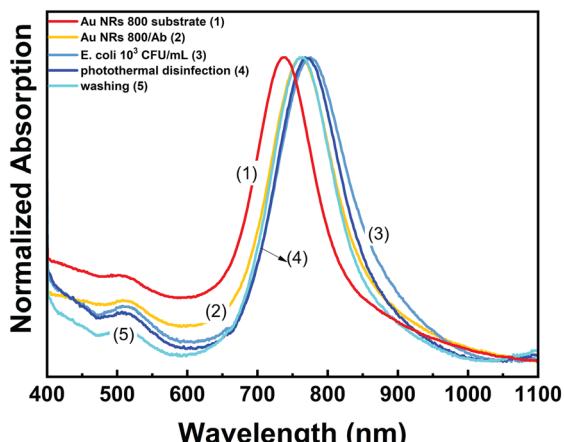
(b)
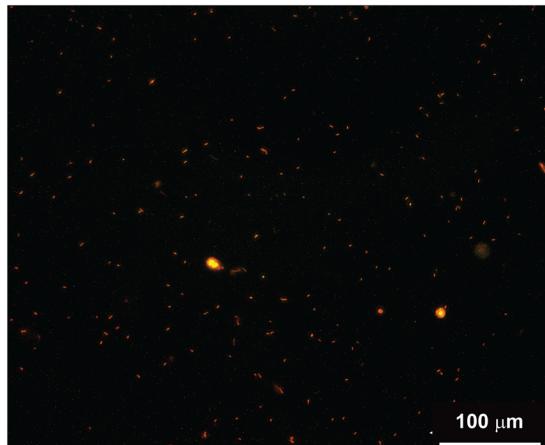
Fig. 9 Photothermal disinfection and reusing of the Au NR 800/Ab substrate. (a) Step-by-step spectroscopic characterization, including Au NR 800 substrate preparation (track/spectrum 1, red), bioactivation (track/spectrum 2, yellow), spectroscopic recognition of *E. coli* (track/spectrum 3, light blue), photothermal experiment (track/spectrum 4, dark blue), and washing step (track/spectrum 5, cyan). After the washing step, the absorption spectrum of the sample overlaps the absorption spectrum of the Au NR 800/Ab substrate, indicating the possibility of reutilizing the biosensor after a suitable washing procedure. (b) Fluorescence microscopy image of the Au NR 800/Ab after the photothermal disinfection experiment, highlighting the presence of nonviable *E. coli* cells by using propidium iodide as a staining agent.

maximum temperature value of 53.8 °C that is sufficient to produce a decrease of *E. coli* cell viability as demonstrated by a previous investigation.[69]

Accordingly, these experimental conditions were employed to assess the ability of the Au NR 800/Ab substrates to perform photothermal disinfection. To this end, the Au NR 800/Ab sample (Fig. 9a, track 2) was incubated for 20 min in a 10^3 CFU mL^{-1} *E. coli* dispersion. After the washing and the drying steps, the absorption spectrum was recorded (Fig. 9a, track 3). As expected, a red-shift of 13 nm was measured. The photothermal disinfection experiment was performed following the procedure reported in the "Multicolor photothermal measurements" section, while the utilized opti-

cal setup is shown in Fig. 8a. The Au NR 800/Ab sample incubated with *E. coli* dispersion was irradiated for 2 min at 808 nm with the CW laser at a power density of 29 W cm^{-2}, thus reaching a maximum temperature of 54 °C. Subsequently, a solution containing 2 μL of propidium iodide was introduced, and the sample was left to incubate for 10 min in the dark, with an additional washing and drying step.

Subsequently, the sample was analysed by fluorescence microscopy. The microscopy analysis reported in Fig. 9b shows red spots of elongated shape uniformly distributed on the surface of the biofunctionalized plasmonic substrate. These are associated with dead *E. coli* cells stained by propidium iodide. Accordingly, we can assert that the investigated experimental conditions are suitable for achieving photothermal disinfection. However, as reported in track 4 of Fig. 9a, the photothermal disinfection step determined a blue shift of 4 nm of the LSPRl without altering the absorption spectrum profile. At this stage, the substrate was washed three times with a NaCl solution to remove cells, rinsed with water, and dried under a nitrogen flow before collecting the absorption spectrum. The result, reported in track 5 of Fig. 9a, shows that the spectroscopic profile of the substrate (presence of the two LSPR bands, absorption intensity ratio between the two LSPRs and FWMH) remained unaltered after the entire procedure. Remarkably, track 5 of Fig. 9a overlaps track 2 of Fig. 9a, namely the absorption spectrum of the as-prepared Au NR 800/Ab substrate. These additional experiments pointed out that the photothermal heating conditions are suitable to induce *E. coli* cell killing and that the substrate is ready to be reused for other experiments.

Therefore, the ability of the Au NR800/Ab substrates to suppress the detected bacteria accumulated on the active surface can prevent the undesired release of pathogens in the environment, thus preventing unintentional pollution. Moreover, a suitable washing procedure enables the reuse of the functionalized substrate, thus reducing the costs associated with its production and making the proposed biosensor sustainable from both an environmental and an economic standpoint.

Conclusions

We have reported a truly innovative label-free and reusable LSPR biosensor for the spectroscopic detection of *E. coli* cells in water. The biosensor consists of an Au NR array immobilized on a glass substrate by the immersive LbL electrostatic assembly method and then bioactivated with a specific antibody incorporated by physisorption. The fabrication of the Au NR array was realized starting from a detailed propaedeutic investigation on Au NR-based bioconjugates in a water dispersion. This preliminary step demonstrated the effectiveness of the antibody in recognizing *E. coli* cells following the antigen/antibody interaction, and the capability of this interaction to cause an alteration of the local *n*, with a consequent shift of the LSPRl dependent on the *E. coli* cell concentration. Moreover, the experimental results allowed us to select Au NR 800 as a plasmonic optical transducer, whose

This journal is © The Royal Society of Chemistry 2022

Environ. Sci.: Nano, 2022, **9**, 3343–3360 | **3357**

morphology is suited to fabricate a LSPR biosensor on a glass substrate. Hence, the resulting Au NR array showed an optimal morphology, maximizing the surface available for antibody incorporation and *E. coli* cell interaction along with excellent optical properties and a bulk sensitivity of 456 nm per refractive index unit. Indeed, the resulting label-free antibody-functionalized Au NR array was able to capture and spectroscopically recognize *E. coli* cells with a LOD of 8.4 CFU mL^{-1} and a response time in a range of a few minutes.

Sensing experiments performed on *S. Thyphimurium* evidenced the biosensor specificity. Furthermore, the Au NR array can generate a broadband thermoplasmonic heating sufficient for inducing the inactivation of *E. coli* cells. After the photothermal disinfection step and a suitable washing procedure, the Au NR 800/Ab substrate is ready to be reused for other experiments. Therefore, the proposed Au NR array offers a green and sustainable perspective for developing next-generation biosensors beyond the biosensing effectiveness. Indeed, the preparation protocol does not require hazardous chemicals, the undesired release of pathogens is avoided, and the Au NR array can be reused, thus representing an outstanding solution regarding environmental impact and solar light-based applications.

Author contributions

F. P. designed the methodology, performed the investigation, carried out the formal analysis of data, and wrote the paper. D. D. B. provided and prepared the bacterial culture. V. V. fabricated the substrates and performed the optical and thermoplasmonic characterization. F. Z. fabricated the substrates and performed the *E. coli* sensing experiments. S. L. and K. J. performed AFM and SEM analysis. S. M. performed the TEM analysis. V. P. analysed the TEM micrographs. V. S. conducted the photoluminescence characterization. N. G., D. E., and M. McC. provided input on the sample preparation and characterization. L. D. S. conceived and formulated the idea, supervised the project, and wrote the manuscript. All the authors discussed the results and revised the manuscript.

Conflicts of interest

There are no conflicts to declare.

Acknowledgements

References

1 W. H. O. (WHO), Drinking-water, https://www.who.int/newsroom/fact-sheets/detail/drinking-water#:~:text=Water%20and%20health,A%2C%20typhoid%2C%20and%20polio, (accessed 21 January, 2022).

2 L. Rizzo, W. Gernjak, P. Krzeminski, S. Malato, C. S. McArdell, J. A. S. Perez, H. Schaar and D. Fatta-Kassinos, Best available technologies and treatment trains to address current challenges in urban wastewater reuse for irrigation of crops in EU countries, *Sci. Total Environ.*, 2020, **710**, 136312.

3 G. Nichols, I. Lake and C. Heaviside, Climate Change and Water-Related Infectious Diseases, *Atmosphere*, 2018, **9**, 385.

4 A. Nijhawan and G. Howard, Associations between climate variables and water quality in low- and middle-income countries: A scoping review, *Water Res.*, 2022, **210**, 117996.

5 R. Metcalf, D. M. Oliver, V. Moresco and R. S. Quilliam, Quantifying the importance of plastic pollution for the dissemination of human pathogens: The challenges of choosing an appropriate 'control' material, *Sci. Total Environ.*, 2022, **810**, 152292.

6 E. Syranidou and N. Kalogerakis, Interactions of microplastics, antibiotics and antibiotic resistant genes within WWTPs, *Sci. Total Environ.*, 2022, **804**, 150141.

7 E. Janik, M. Ceremuga, J. Saluk-Bijak and M. Bijak, Biological Toxins as the Potential Tools for Bioterrorism, *Int. J. Mol. Sci.*, 2019, **20**, 1181.

8 J. Li, Y. Zhu, X. Wu and M. R. Hoffmann, Rapid Detection Methods for Bacterial Pathogens in Ambient Waters at the Point of Sample Collection: A Brief Review, *Clin. Infect. Dis.*, 2020, **71**, S84–S90.

9 J. Alves, F. A. Sargison, H. Stawarz, W. B. Fox, S. G. Huete, A. Hassan, B. McTeir and A. C. Pickering, A case report: insights into reducing plastic waste in a microbiology laboratory, *Access Microbiol.*, 2021, **3**, 000173.

10 Z. Yang, B. Kasprzyk-Hordern, C. G. Frost, P. Estrela and K. V. Thomas, Community Sewage Sensors for Monitoring Public Health, *Environ. Sci. Technol.*, 2015, **49**, 5845–5846.

11 Z. Guo, Y. Jia, X. Song, J. Lu, X. Lu, B. Liu, J. Han, Y. Huang, J. Zhang and T. Chen, Giant Gold Nanowire Vesicle-Based Colorimetric and SERS Dual-Mode Immunosensor for Ultrasensitive Detection of Vibrio parahemolyticus, *Anal. Chem.*, 2018, **90**(10), 6124–6130.

12 B. De Angelis, N. Depalo, F. Petronella, C. Quintarelli, M. L. Curri, R. Pani, A. Calogero, F. Locatelli and L. De Sio, Stimuli-responsive nanoparticle-assisted immunotherapy: A new weapon against solid tumours, *J. Mater. Chem. B*, 2020, **8**, 1823–1840.

13 S. Eustis and M. A. El-Sayed, Why gold nanoparticles are more precious than pretty gold: Noble metal surface plasmon resonance and its enhancement of the radiative and nonradiative properties of nanocrystals of different shapes, *Chem. Soc. Rev.*, 2006, **35**, 209–217.

14 L. M. Liz-Marzán, Nanometals, *Mater. Today*, 2004, **7**, 26–31.

15 K. M. Mayer and J. H. Hafner, Localized Surface Plasmon Resonance Sensors, *Chem. Rev.*, 2011, **111**, 3828–3857.

16 M. Yüce and H. Kurt, How to make nanobiosensors: surface modification and characterisation of nanomaterials for biosensing applications, *RSC Adv.*, 2017, **7**, 49386–49403.

17 J.-H. Lee, H.-Y. Cho, H. K. Choi, J.-Y. Lee and J.-W. Choi, Application of Gold Nanoparticle to Plasmonic Biosensors, *Int. J. Mol. Sci.*, 2018, **19**, 2021.

3358 | *Environ. Sci.: Nano*, 2022, **9**, 3343–3360

This journal is © The Royal Society of Chemistry 2022

18 S. Y. Oh, N. S. Heo, S. Shukla, H.-J. Cho, A. T. E. Vilian, J. Kim, S. Y. Lee, Y.-K. Han, S. M. Yoo and Y. S. Huh, Development of gold nanoparticle-aptamer-based LSPR sensing chips for the rapid detection of Salmonella typhimurium in pork meat, *Sci. Rep.*, 2017, **7**, 10130.

19 Y. Xu, Z. Luo, J. Chen, Z. Huang, X. Wang, H. An and Y. Duan, Ω-Shaped Fiber-Optic Probe-Based Localized Surface Plasmon Resonance Biosensor for Real-Time Detection of Salmonella Typhimurium, *Anal. Chem.*, 2018, **90**, 13640–13646.

20 P. Halkare, N. Punjabi, J. Wangchuk, S. Madugula, K. Kondabagil and S. Mukherji, Label-Free Detection of Escherichia coli from Mixed Bacterial Cultures Using Bacteriophage T4 on Plasmonic Fiber-Optic Sensor, *ACS Sens.*, 2021, **6**, 2720–2727.

21 R. Funari, N. Bhalla, K.-Y. Chu, B. Söderström and A. Q. Shen, Nanoplasmonics for Real-Time and Label-Free Monitoring of Microbial Biofilm Formation, *ACS Sens.*, 2018, **3**, 1499–1509.

22 S. T. Odonkor and T. Mahami, Escherichia coli as a Tool for Disease Risk Assessment of Drinking Water Sources, *Internet J. Microbiol.*, 2020, **2020**, 2534130–2534130.

23 C. Wang and J. Irudayaraj, Gold Nanorod Probes for the Detection of Multiple Pathogens, *Small*, 2008, **4**, 2204–2208.

24 Q. Chen, L. Zhang, Y. Feng, F. Shi, Y. Wang, P. Wang and L. Liu, Dual-functional peptide conjugated gold nanorods for the detection and photothermal ablation of pathogenic bacteria, *J. Mater. Chem. B*, 2018, **6**, 7643–7651.

25 J. Zhou, F. Tian, R. Fu, Y. Yang, B. Jiao and Y. He, Enzyme–Nanozyme Cascade Reaction-Mediated Etching of Gold Nanorods for the Detection of Escherichia coli, *ACS Appl. Nano Mater.*, 2020, **3**, 9016–9025.

26 R. S. Norman, J. W. Stone, A. Gole, C. J. Murphy and T. L. Sabo-Attwood, Targeted Photothermal Lysis of the Pathogenic Bacteria, Pseudomonas aeruginosa, with Gold Nanorods, *Nano Lett.*, 2008, **8**, 302–306.

27 T. Placido, L. Tognaccini, B. D. Howes, A. Montrone, V. Laquintana, R. Comparelli, M. L. Curri, G. Smulevich and A. Agostiano, Surface Engineering of Gold Nanorods for Cytochrome c Bioconjugation: An Effective Strategy To Preserve the Protein Structure, *ACS Omega*, 2018, **3**, 4959–4967.

28 M. von der Lühe, A. Weidner, S. Dutz and F. H. Schacher, Reversible Electrostatic Adsorption of Polyelectrolytes and Bovine Serum Albumin onto Polyzwitterion-Coated Magnetic Multicore Nanoparticles: Implications for Sensing and Drug Delivery, *ACS Appl. Nano Mater.*, 2018, **1**, 232–244.

29 L.-M. Petrila, F. Bucatariu, M. Mihai and C. Teodosiu, Polyelectrolyte Multilayers: An Overview on Fabrication Properties, and Biomedical and Environmental Applications, *Materials*, 2021, **14**, 4152.

30 Z. Liu, Z. Yan and L. Bai, Layer-by-layer assembly of polyelectrolyte and gold nanoparticle for highly reproducible and stable SERS substrate, *Appl. Surf. Sci.*, 2016, **360**, 437–441.

31 J. J. Richardson, M. Björnmalm and F. Caruso, Technology-driven layer-by-layer assembly of nanofilms, *Science*, 2015, **348**, aaa2491.

32 T. Placido, E. Fanizza, P. Cosma, M. Striccoli, M. L. Curri, R. Comparelli and A. Agostiano, Electroactive Layer-by-Layer Plasmonic Architectures Based on Au Nanorods, *Langmuir*, 2014, **30**, 2608–2618.

33 Q. Yang, G. Zhu, L. Singh, Y. Wang, R. Singh, B. Zhang, X. Zhang and S. Kumar, Highly sensitive and selective sensor probe using glucose oxidase/gold nanoparticles/graphene oxide functionalized tapered optical fiber structure for detection of glucose, *Optik*, 2020, **208**, 164536.

34 Y. Ziai, F. Petronella, C. Rinoldi, P. Nakielski, A. Zakrzewska, T. A. Kowalewski, W. Augustyniak, X. Li, A. Calogero, I. Sabała, B. Ding, L. De Sio and F. Pierini, Chameleon-inspired multifunctional plasmonic nanoplatforms for biosensing applications, *NPG Asia Mater.*, 2022, **14**, 18.

35 A. Vitalone, A. Di Sotto, C. L. Mammola, R. Heyn, S. Miglietta, P. Mariani, F. Sciubba, F. Passarelli, P. Nativio and G. Mazzanti, Phytochemical analysis and effects on ingestive behaviour of a Caralluma fimbriata extract, *Food Chem. Toxicol.*, 2017, **108**, 63–73.

36 M. Relucenti, S. Miglietta, G. Bove, O. Donfrancesco, E. Battaglione, P. Familiari, C. Barbaranelli, E. Covelli, M. Barbara and G. Familiari, SEM BSE 3D Image Analysis of Human Incus Bone Affected by Cholesteatoma Ascribes to Osteoclasts the Bone Erosion and VpSEM dEDX Analysis Reveals New Bone Formation, *Scanning*, 2020, 9371516.

37 M. H. Jazayeri, H. Amani, A. A. Pourfatollah, H. Pazoki-Toroudi and B. Sedighimoghaddam, Various methods of gold nanoparticles (GNPs) conjugation to antibodies, *Sens. Bio-Sens. Res.*, 2016, **9**, 17–22.

38 X. Huang, I. H. El-Sayed, W. Qian and M. A. El-Sayed, Cancer Cell Imaging and Photothermal Therapy in the Near-Infrared Region by Using Gold Nanorods, *J. Am. Chem. Soc.*, 2006, **128**, 2115–2120.

39 Y. Zhu, C. Qu, H. Kuang, L. Xu, L. Liu, Y. Hua, L. Wang and C. Xu, Simple, rapid and sensitive detection of antibiotics based on the side-by-side assembly of gold nanorod probes, *Biosens. Bioelectron.*, 2011, **26**, 4387–4392.

40 P. Hao, Y. Wu and F. Li, Improved sensitivity of wavelength-modulated surface plasmon resonance biosensor using gold nanorods, *Appl. Opt.*, 2011, **50**, 5555–5558.

41 S. P. R. Kobaku, C. S. Snyder, R. G. Karunakaran, G. Kwon, P. Wong, A. Tuteja and G. Mehta, Wettability Engendered Templated Self-Assembly (WETS) for the Fabrication of Biocompatible, Polymer–Polyelectrolyte Janus Particles, *ACS Macro Lett.*, 2019, **8**, 1491–1497.

42 K. Achazi, R. Haag, M. Ballauff, J. Dernedde, J. N. Kizhakkedathu, D. Maysinger and G. Multhaup, Understanding the Interaction of Polyelectrolyte Architectures with Proteins and Biosystems, *Angew. Chem., Int. Ed.*, 2021, **60**, 3882–3904.

43 P. Garidel, M. Hegyi, S. Bassarab and M. Weichel, A rapid, sensitive and economical assessment of monoclonal antibody conformational stability by intrinsic tryptophan fluorescence spectroscopy, *Biotechnol. J.*, 2008, **3**, 1201–1211.

This journal is © The Royal Society of Chemistry 2022

Environ. Sci.: Nano, 2022, **9**, 3343–3360 | **3359**

44 R. T. Busch, F. Karim, J. Weis, Y. Sun, C. Zhao and E. S. Vasquez, Optimization and Structural Stability of Gold Nanoparticle–Antibody Bioconjugates, *ACS Omega*, 2019, **4**, 15269–15279.

45 Y. Zhang, J. L. Y. Wu, J. Lazarovits and W. C. W. Chan, An Analysis of the Binding Function and Structural Organization of the Protein Corona, *J. Am. Chem. Soc.*, 2020, **142**, 8827–8836.

46 A. K. Singh, D. Senapati, S. Wang, J. Griffin, A. Neely, P. Candice, K. M. Naylor, B. Varisli, J. R. Kalluri and P. C. Ray, Gold Nanorod Based Selective Identification of Escherichia coli Bacteria Using Two-Photon Rayleigh Scattering Spectroscopy, *ACS Nano*, 2009, **3**, 1906–1912.

47 R. Das, K. K. Paul and P. K. Giri, Highly sensitive and selective label-free detection of dopamine in human serum based on nitrogen-doped graphene quantum dots decorated on Au nanoparticles: Mechanistic insights through microscopic and spectroscopic studies, *Appl. Surf. Sci.*, 2019, **490**, 318–330.

48 O. Yavas, M. Svedendahl, P. Dobosz, V. Sanz and R. Quidant, On-a-chip Biosensing Based on All-Dielectric Nano-resonators, *Nano Lett.*, 2017, **17**, 4421–4426.

49 N. A. Masdor, Detection Limit of the Four-Parameter Logistic Model for the Quantitative Detection of Serum Squamous Cell Carcinoma Antigenin Cervical Cancer Based on Surface Plasmon Resonance Biosensor, *Journal of Environmental Microbiology and Toxicology*, 2021, **9**, 30–32.

50 M. Lu, H. Zhu, C. G. Bazuin, W. Peng and J.-F. Masson, Polymer-Templated Gold Nanoparticles on Optical Fibers for Enhanced-Sensitivity Localized Surface Plasmon Resonance Biosensors, *ACS Sens.*, 2019, **4**, 613–622.

51 C. Daengngam, S. Lethongkam, P. Srisamran, S. Paosen, P. Wintachai, B. Anantravanit, V. Vattanavanit and S. Voravuthikunchai, Green fabrication of anti-bacterial biofilm layer on endotracheal tubing using silver nanoparticles embedded in polyelectrolyte multilayered film, *Mater. Sci. Eng., C*, 2019, **101**, 53–63.

52 T. Kruk, M. Gołda-Cępa, K. Szczepanowicz, L. Szyk-Warszyńska, M. Brzychczy-Włoch, A. Kotarba and P. Warszyński, Nanocomposite multifunctional polyelectrolyte thin films with copper nanoparticles as the antimicrobial coatings, *Colloids Surf., B*, 2019, **181**, 112–118.

53 E. V. Lengert, S. I. Koltsov, J. Li, A. V. Ermakov, B. V. Parakhonskiy, E. V. Skorb and A. G. Skirtach, Nanoparticles in Polyelectrolyte Multilayer Layer-by-Layer (LbL) Films and Capsules—Key Enabling Components of Hybrid Coatings, *Coatings*, 2020, **10**, 1131.

54 E. Guzmán, H. A. Ritacco, F. Ortega and R. G. Rubio, Growth of Polyelectrolyte Layers Formed by Poly(4-styrenesulfonate sodium salt) and Two Different Polycations: New Insights from Study of Adsorption Kinetics, *J. Phys. Chem. C*, 2012, **116**, 15474–15483.

55 E. Guzmán, R. G. Rubio and F. Ortega, A closer physico-chemical look to the Layer-by-Layer electrostatic self-assembly of polyelectrolyte multilayers, *Adv. Colloid Interface Sci.*, 2020, **282**, 102197.

56 Y. Bao, L. Vigderman, E. R. Zubarev and C. Jiang, Robust Multilayer Thin Films Containing Cationic Thiol-Functionalized Gold Nanorods for Tunable Plasmonic Properties, *Langmuir*, 2012, **28**, 923–930.

57 K. M. Mayer, S. Lee, H. Liao, B. C. Rostro, A. Fuentes, P. T. Scully, C. L. Nehl and J. H. Hafner, A Label-Free Immunoassay Based Upon Localized Surface Plasmon Resonance of Gold Nanorods, *ACS Nano*, 2008, **2**, 687–692.

58 B. Nikoobakht and M. A. El-Sayed, Surface-Enhanced Raman Scattering Studies on Aggregated Gold Nanorods, *J. Phys. Chem. A*, 2003, **107**, 3372–3378.

59 F. Bruyneel, H. De Smet, J. Vanfleteren and A. Van Calster, Method for measuring the cell gap in liquid-crystal displays, *Opt. Eng.*, 2001, **40**, 259–267.

60 B. Špačková, P. Wrobel, M. Bocková and J. Homola, Optical Biosensors Based on Plasmonic Nanostructures: A Review, *Proc. IEEE*, 2016, **104**, 2380–2408.

61 L. Song, L. Zhang, Y. Huang, L. Chen, G. Zhang, Z. Shen, J. Zhang, Z. Xiao and T. Chen, Amplifying the signal of localized surface plasmon resonance sensing for the sensitive detection of Escherichia coli O157:H7, *Sci. Rep.*, 2017, **7**, 3288.

62 L. Tian, E. Chen, N. Gandra, A. Abbas and S. Singamaneni, Gold Nanorods as Plasmonic Nanotransducers: Distance-Dependent Refractive Index Sensitivity, *Langmuir*, 2012, **28**(50), 17435–17442.

63 M. Piliarik, P. Kvasnička, N. Galler, J. R. Krenn and J. Homola, Local refractive index sensitivity of plasmonic nanoparticles, *Opt. Express*, 2011, **19**(10), 9213–9922.

64 O. Saison-Francioso, G. Lévêque, A. Akjouj, Y. Pennec, B. Djafari-Rouhani, S. Szunerits and R. Boukherroub, Plasmonic Nanoparticles Array for High-Sensitivity Sensing: A Theoretical Investigation, *J. Phys. Chem. C*, 2012, **116**(33), 17819–17827.

65 T. Rindzevicius, Y. Alaverdyan, M. Käll, W. A. Murray and W. L. Barnes, Long-Range Refractive Index Sensing Using Plasmonic Nanostructures, *J. Phys. Chem. C*, 2007, **111**(32), 11806–11810.

66 A. D. McNaught, *Compendium of chemical terminology*, vol. 1669, Blackwell Science, Oxford, 1997.

67 A. O. Govorov and H. H. Richardson, Generating heat with metal nanoparticles, *Nano Today*, 2007, **2**, 30–38.

68 L. Song, N. Qiu, Y. Huang, Q. Cheng, Y. Yang, H. Lin, F. Su and T. Chen, Macroscopic Orientational Gold Nanorods Monolayer Film with Excellent Photothermal Anticounterfeiting Performance, *Adv. Opt. Mater.*, 2020, **8**, 1902082.

69 F. Annesi, A. Pane, M. A. Losso, A. Guglielmelli, F. Lucente, F. Petronella, T. Placido, R. Comparelli, M. G. Guzzo, M. L. Curri, R. Bartolino and L. De Sio, Thermo-plasmonic killing of Escherichia coli TG1 bacteria, *Materials*, 2019, **12**, 1530.

3360 | *Environ. Sci.: Nano*, 2022, **9**, 3343–3360

This journal is © The Royal Society of Chemistry 2022